



UNIVERSITY OF UTRECHT

DEBYE INSTITUTE

NANOPHOTONICS GROUP

---

# Čerenkov Wakes in Ultra-Cold Sodium Gases

---

*Author:*  
Guanqiao Li

*Supervisors:*  
Prof. Dr. Peter van der Straten

July 14, 2016



## Abstract

In classical (normal) fluids when an object moves faster than the speed of sound it creates wake patterns in the form of cones. This phenomenon was also observed in superfluid Bose-Einstein condensates by Cornell [1]. We will redo these experiments using a tightly focused blue detuned laser and moving atomic cloud. Wake formations of both the superfluid and the classical fluid are observed simultaneously in our experiments. These measured angles will be compared with the corresponding angles predicted by theory with a determined speed of sound of 4.8 mm/s. The wake angles generated in the superfluid correspond with theory for an expected speed of sound of 4.8 mm/s. The wake angles generated in the normal fluid however correspond with theory for an unexpected speed of sound of 77 mm/s. We have also extended the existing theory on the formation of supersonic wakes for finite potential barriers. The results predict that the size and speed of the barrier with respect to the condensate will start to suppress higher order wake patterns.



---

## Contents

<b>1</b>	<b>Introduction</b>	<b>1</b>
1.1	Bose-Einstein Condensate . . . . .	1
1.2	Superfluidity . . . . .	2
1.3	Čerenkov Effect . . . . .	2
1.4	Thesis Outline . . . . .	3
<b>2</b>	<b>Bose-Einstein Condensate of Sodium</b>	<b>4</b>
2.1	Sodium Atoms . . . . .	4
2.2	Laser System . . . . .	4
2.3	Dark Spot Magneto-Optical Trap . . . . .	5
2.4	Evaporative Cooling in the Magnetic Trap . . . . .	6
2.5	Imaging . . . . .	7
2.5.1	Absorption Imaging . . . . .	7
2.5.2	Phase-Contrast Imaging . . . . .	9
<b>3</b>	<b>Supersonic Flow</b>	<b>11</b>
3.1	Sonic Speed Limit . . . . .	11
3.2	Gaussian Barrier Setup . . . . .	12
3.2.1	Gaussian Beam Optics . . . . .	14
3.2.2	Atom-Laser Interaction . . . . .	15
3.3	Oscillations in the Magnetic Trap . . . . .	17
3.4	Measurements . . . . .	21
<b>4</b>	<b>Čerenkov Wakes</b>	<b>22</b>
4.1	Bogoliubov-Čerenkov Theory . . . . .	22
4.2	Gaussian Potential . . . . .	26

4.3	Measurements . . . . .	27
<b>5</b>	<b>Discussions</b>	<b>35</b>
5.1	Discussion . . . . .	35
5.2	Conclusion . . . . .	36
5.3	Outlook . . . . .	36
	<b>Appendix A : The Linear Bogoliubov Approximation</b>	<b>38</b>
	<b>Appendix B : Čerenkov Condition In BEC</b>	<b>40</b>
	<b>References</b>	<b>42</b>
<b>A</b>	<b>Acknowledgements</b>	<b>44</b>

# 1 Introduction

The first Bose-Einstein Condensates (BEC) was realized experimentally in 1995 with rubidium, lithium, and sodium (later awarded the Nobel price in 2001 [2], [3]) 70 years after the publication of the paper in which Albert Einstein theoretically predicted this new phase using the same method Satyendra Nath Bose used for the quantum statistics of photons. When a boson gas reach a critical temperature under a certain density the atoms start to fall to the lowest available ground state. The atoms that macroscopically occupy the ground state condenses to a new quantum phase called Bose-Einstein Condensate. In this phase each individual wavefunction starts to overlap to form one single wavefunction, thus allowing for experiments on the phenomena of quantum mechanics on a macroscopic scale.

## 1.1 Bose-Einstein Condensate

In the classical picture particles in a gas move randomly with respect to each other with large velocity. When a gas is cooled down and its density increases one would expect that it would undergo two classical phase transitions, namely the transition from gas to fluid and fluid to solid. Albert Einstein however published a paper in 1924 where he applied the method used by Satyendra Nath Bose on photon gas to a bosonic gas. Here he discovered that an ideal bosonic gas has a critical temperature and density, when reached the system starts to condensate into a new quantum phase where the atoms will macroscopically occupy the ground state. This is possible due to a fundamental property bosons have which is the symmetry under the interchange of two bosons, which gives rise to the Bose-Einstein distribution:

$$f(\epsilon_k) = \frac{1}{e^{(\epsilon_k - \mu)/k_B T} - 1}. \quad (1.1)$$

Here  $\epsilon_k$  is the energy of a single-particle state of momentum  $k$ ,  $\mu$  is the chemical potential,  $T$  is the temperature, and  $k_B$  is the Boltzmann constant. The transition temperature for a non-interacting Bose gas can be calculated with the condition that all atoms can be accommodated in excited states and  $\mu = 0$ . The result is the critical temperature given as  $k_B T_c \approx 0.94 \hbar (\omega_x \omega_y \omega_z N)^{1/3}$  for atoms in a 3D harmonic-oscillator potential with  $\omega_x$ ,  $\omega_y$ , and  $\omega_z$  corresponding to the trapping frequency of the potential in the x, y, and z direction respectively.

In this regime inter-particle distances are of the same order as the de Broglie wavelength given as:

$$\Lambda_T = \sqrt{\frac{2\pi\hbar^2}{mk_B T}}. \quad (1.2)$$

Here  $\hbar$  is the reduced Planck constant and  $m$  is the mass of the sodium atom. Atoms

can be viewed as matter waves where the distance between each other is so small that the matter wave begin to overlap into one single matter wave. The phase-space density  $\Phi$  which is defined as the number of atoms consisting in a volume  $\Lambda_T$  is expressed as

$$\Phi = n(\mathbf{r})\Lambda_T^3 \approx 1. \quad (1.3)$$

Then for the inter-particle distance to reach the regime of the de Broglie wavelength the phase-space density must reach approximately unity. Eq. 1.3 shows that the only free parameters are the density  $n(\mathbf{r})$  and the temperature  $T$ , where  $n(\mathbf{r})$  goes linearly and  $T$  goes to the power of  $-3/2$  making the temperature the more favorable one to manipulate. This does not mean the density can be ignored, the density must be in a region where it is not too large that it goes to the liquid or solid phase or too small where the critical temperature goes to 0.

## 1.2 Superfluidity

One of the interesting phenomena in a BEC is superfluidity. The criteria for calling a behavior superfluid is historically based on the behavior of the phase of  $^4\text{He}$  below  $T_\lambda$  called He-II. Some important differences of a superfluid compared to a normal fluid are the existence of quantized vortices in a rotated system and frictionless flow up to a critical velocity, below this critical velocity no modes are excited. This velocity is also known as the Landau critical velocity derived by Lev Davidovich Landau. He determined that if the gradient of the excitation spectrum  $\epsilon(p)$  for a momentum  $p$  has a nonzero minimum, than that value is defined as the critical velocity below which no modes can be excited:

$$v_c = \min \left( \frac{\epsilon_p}{p} \right) \neq 0. \quad (1.4)$$

For pure phonon excitations at zero temperature the critical velocity is equal to the Bogoliubov speed of sound. The existence of a critical velocity in a sodium BEC is know to exist and was also observed [4].

## 1.3 Čerenkov Effect

In the classical case when a object moves through a medium at supersonic speeds it creates a density modulation in the shape of a cone where the aperture is dependent on the Mach number  $M$  as  $\sin(\phi) = c/v = 1/M$ . Analogous to this is the Čerenkov

effect for charged particle moving through a dielectric medium faster than the phase velocity of light in that medium. This results in the emission of light moving orthogonal with respect to the cone surface where the aperture behaves the same as for the Mach cone with  $c$  as the group velocity. By applying the theory of Čerenkov radiation onto a superfluid with excitations according to the Bogoliubov dispersion relation one can produce wave patterns that are analogous to the Mach cone.

## 1.4 Thesis Outline

This thesis contains the Bogoliubov-Čerenkov theory describing wakes in BECs at the supersonic region. These phenomenons are experimentally observed. First a short introduction on the type of atom (sodium) and the method of creating a BEC and imaging it is discussed in chapter 2. Chapter 3 will start with the discussion on the speed of sound in a BEC. Next it will discuss the the setup to create a potential barrier for the experiment and the interactions between atom and light. It will continue onto the discussion of moving the BEC with different velocities using the magnetic fields that traps the atomic cloud (see Sec. 2.3 and 2.4). The measured velocities are shown in the final section of chapter 3. Chapter 4 will start with the introduction to the Bogoliubov-Čerenkov theory with a delta-potential as barrier. Next a Gaussian potential is applied to the theory and in the last section results are presented from the wake experiments. Chapter 5 will start with discussing the results of the wake experiments followed by the conclusions and it will end with an outlook.

## 2 Bose-Einstein Condensate of Sodium

The recipe to create a gas cloud cold and dens enough to start a condensation to the Bose-Einstein quantum phase is to first create a beam of sodium gas using a recirculating oven containing a solid block of pure sodium, then by slowing the average speed of the atoms in the beam down by shining resonant laser light from opposite direction to the beam. After having slowed the atoms down to the order of 40 m/s, they are confined in a dark spot Magneto-Optical Trap (MOT) which is a combination of laser light detuned from resonance and a quadrupole magnetic field. The atoms are then transferred to a Magnetic Trap (MT) and a technique called evaporative cooling is applied. This final process cools the cloud down to below the critical temperature where the system will start to condense. Finally two imaging methods are used to detect the results from the BEC, namely absorption imaging and phase-contrast imaging (PCI).

### 2.1 Sodium Atoms

For the experiment  $^{23}\text{Na}$  atoms will be used and the focus will on the transitions between the hyperfine structures of the levels  $3^2\text{S}_{1/2}$  and  $3^2\text{P}_{3/2}$  state which are detuned from each other by 589.2 nm (508.8 THz). The  $3^2\text{S}_{1/2}$  ground state also has a hyperfine splitting of  $F_g = 1, 2$  due to the nuclear spin and electron angular momentum coupling. The  $3^2\text{P}_{3/2}$  excited state has a hyperfine splitting of  $F_e = 0, 1, 2, 3$ . The detuning between the hyperfine states are found in Ref. [5]. The important transitions for cooling sodium atoms is the closed cycling transition  $3^2\text{S}_{1/2}, F_g = 2 \rightarrow 3^2\text{P}_{3/2}, F_e = 3$  and the repumping transition  $3^2\text{S}_{1/2}, F_g = 1 \rightarrow 3^2\text{P}_{3/2}, F_e = 2$ . The repumping is necessary, because of the small splitting of the hyperfine levels in the  $3^2\text{P}_{3/2}$  state there is a slight change that atoms will excite to the  $F_e = 2$  level due to off-resonant scattering and then fall to the  $3^2\text{S}_{1/2}, F_g = 1$  state. This happens where the magnetic field is nearly zero which is at the zero-crossing of the Zeeman slower and at the center of the MOT (see Sec. 2.3).

To cool sodium atoms one must first heat it to a temperature of 300 °C. This is done in the oven where the atoms will reach speeds up to 800 m/s. The atoms will therefore exit the oven at large velocity through two diaphragms that will collimate the atomic beam. It will next enter the Zeeman slower where the coils will generate a magnetic field such that it shifts the hyperfine state according to the Doppler shift that the atom at a specific speed is experiencing, therefore the stream of atoms stays resonant with the laser light. When the atoms exit the Zeeman slower and enter the main experimental chamber with a velocity in the order of 10 m/s they will be trapped in the MOT which is in the center of the chamber.

### 2.2 Laser System

As mentioned in the previous section, in order to slow sodium atoms at large velocities one need to excite them from their ground state to an excited state. A laser

Beam	Power
MOT XY	34 mW
MOT Z	14 mW
MOT repumper	5 mW
Zeeman	120 mW
Zeeman repumper	15 mW
Spin polarizer	2 mW
Probe (side)	0.012 mW
Probe (top)	0.12 mW

**Table 2.1:** The power of each laser beam needed. The MOT XY, Z, and Zeeman are split from the TA-SHG Pro 14095 laser. The other ones are split from the TA-SHG Pro 14074.

system that is able to generate a precise frequency that locks on that exact excitation frequency is therefore essential to the cooling process. A schematic sketch of the most recent setup of the laser system can be found in Ref. [6]. The complete system consist of two Toptica TA-SHG Pro diode lasers each able to deliver up to 1.2 W of power at the wavelength of 589 nm with a linewidth below 500 kHz. For a full description on the diode laser, see Ref. [7]. The frequency of the lasers are locked onto specific atomic hyperfine transitions using the saturated absorption spectroscopy method with a sodium vapor cell reference. The TA-SHG Pro 14095 laser is locked to the  $F_g = 2 \rightarrow F_e = 3$  transition which will be used for the generating the cycling transition light for the MOT XY and Z beam (See Sec. 2.3) and the Zeeman slower beam (see Sec. 2.1). The TA-SHG Pro 14074 laser is locked to the  $F_g = 1 \rightarrow F_e = 1, 2$  crossover which will be used for generating the probe (see Sec. 2.5, spin polarization (see Sec. 2.4), and repumping transition light (see Ref. 2.1). Table 2.1 shows how much power goes into each beam path.

### 2.3 Dark Spot Magneto-Optical Trap

The diode lasers are placed on a separate optical table and each beam path is coupled to an optical fiberport. The beam is directed via polarization-maintaining single mode fiber optic patch cables to their designated positions on the main experimental table containing the high vacuum chamber, Zeeman slower, and oven.

When the atoms enter the ultra-high vacuum chamber it would have reached velocities below the capture velocity of the MOT of around 40 m/s. The basic principle of a MOT is to trap a cloud of atoms by having three retro-reflecting laser beams, each orthogonal with respect to the other, that is detuned below the cycling transition frequency and a quadrupole magnetic field. The combination of the magnetic field inducing a Zeeman shift and an atom moving away from the MOT center inducing a Doppler shift will result to radiation pressure that will cool and confine the atoms. A extra feature that is added compared to a traditional bright MOT is an extra beam

containing a hole in the middle that is resonant with the repumping transition. The idea behind this feature is containing atoms that have fallen to the  $F_g = 1$  ground state. The  $F_g = 1$  is a dark state due to their invisibility to the cycling light of the MOT. Because the density of a bright MOT is limited due to light-assisted inelastic two-body collisions and ground state atoms that re-absorb emitted photons which create a repulsive force. It is possible to exceed the limitation in the density of the bright MOT by implementing the dark state atoms. The atoms in the dark state experience a reduced radiation pressure in the dark spot and this reduces the losses in the dark spot MOT.

## 2.4 Evaporative Cooling in the Magnetic Trap

The atoms in the dark spot MOT are cooled by the Doppler cooling mechanism, this mechanism has a temperature limit called the Doppler temperature where it can not go below. Since the temperature limit is still far to large for Bose-Einstein condensation to take place another method is needed to cool further towards the critical temperature. Evaporative cooling is used as the next cooling method to reach the critical temperature.

After the dark spot MOT is loaded the atoms are transferred to the MT generated by the coils in a cloverleaf configuration for radial trapping and pinch-bias coils for axial trapping. In the MOT all three magnetic sub-states  $m_F = -1, 0, 1$  of the  $F_g = 1$  are confined. But due to nature of those three sub-states and their interaction with a magnetic field, only one sub-state can be trapped magnetically. Atoms in the  $m_F = 0$  sub-state does not interact with the magnetic field, the  $m_F = 1$  state are high field seekers and the  $m_F = -1$  state are low field seekers. Since the MT creates a field minimum near the center of the vacuum chamber, it can only trap atoms that are in the  $m_F = -1$  sub-state. This yields to having a transition efficiency of 33%. To increase this one must apply a method called spin polarization where a beam of  $\sigma^-$  polarized resonant light is shone onto the cloud for 700 ms under a strong magnetic field. This will effectively pump atoms from the  $m_F = 0, 1$  state to the  $m_F = -1$  sub-state. The method yields a number increase of up to 50% in the MT.

After transitioning the atoms to the MT, the final cooling procedure will be executed. The technique evaporative cooling as the name implies cools the system by "evaporating" the hotter atoms. The experimental setup comprises of a well-placed antenna that generates a radio-frequency signal that induces a spin-flip onto the atoms forcing the transition  $F_g = 1, m_F = -1 \rightarrow F_g = 1, m_F = 0, 1$ . The most important feature of this method is that it is energy selective. This means that the resonant frequency is proportional to the magnetic field:

$$g_L \mu_B m_F |B(\mathbf{r})| = \hbar \omega_{\text{rf}}. \quad (2.1)$$

Here  $g_L$  is the Landé g-factor,  $\mu_B$  is the Bohr magneton, and  $\omega_{\text{rf}}$  is the radio fre-

quency. Since the energy of the atom is also proportional to the magnetic field as  $E = g_L \mu_B m_F |B(\mathbf{r}) - B(0)|$  one can selectively expel the atoms in the higher energy state from the MT. By lowering the frequency more atom of the energy  $E > \hbar |m_F| (\omega_{\text{rf}} - \omega_0)$  are expelled, where  $\omega_0$  is the frequency correspondent to the bottom of the MT. This forces the whole system to rethermalize resulting to a net increase of density and decrease in temperature.

## 2.5 Imaging

There is currently two methods available to image the cloud, namely absorption imaging and PCI. There are two beam paths for the probe beam to travel, which path the probe beam travels can be switch via a mirror on a flippable mount. This results to two imaging angles, namely side imaging and top imaging. For side imaging the probe beam passes the cloud from an angle with respect from the horizontal plane, it has a demagnification factor of 2.7. For top imaging the probe beam passes the cloud from the top, it has a magnification factor of 3.

### 2.5.1 Absorption Imaging

Absorption imaging can be applied in both side and top imaging. The method is based on the principle of shining resonant light onto the cloud therefore casting a shadow onto the camera due to the absorption of photons. By exposing the cloud to resonant light, it gets destroyed due to all the atoms being excited from its ground state therefore it is impossible to take multiple pictures of the same BEC.

The imaging procedure consists of three pictures: one of the atomic cloud  $I_{\text{atoms}}$ , one of only the probe light  $I_{\text{probe}}$ , and one with only the background light  $I_{\text{background}}$ . The transmittance  $I/I_0$ , which is the quantity of the normalized picture of the cloud, can be calculated by applying the Lambert-Beer law:

$$\begin{aligned} \frac{I}{I_0} &= \frac{I_{\text{atoms}} - I_{\text{background}}}{I_{\text{probe}} - I_{\text{background}}} \\ &= e^{-\text{OD}}. \end{aligned} \tag{2.2}$$

The optical density (OD) is related to the density distribution of the atomic cloud by the following equation:

$$\text{OD} = \sigma n_{\text{column}}. \tag{2.3}$$

Here  $\sigma$  is the cross section  $\sigma = C_{g,e} \frac{3\lambda^2}{2\pi}$  with  $C_{g,e}$  as the relative transition strength and  $\lambda$  as the wavelength of the probe light.  $\text{OD}$  is a 2D image of a 3D cloud this

means that  $n_{\text{column}}$  is the column density which is a 2D density distribution with the dimension of depth integrated out. The column density for the thermal and condensate in a cigar shaped trap is

$$n_{\text{th}}(r, z, t) = \frac{mk_{\text{B}}^2 T^2}{2\pi\omega_r \hbar^3 (1 + \omega_r^2 t^2)^{3/2} (1 + \omega_z^2 t^2)} g_2 \left[ e^{\frac{\mu}{k_{\text{B}} T} - \frac{r^2}{x_{r,\text{th}}^2} - \frac{z^2}{x_{z,\text{th}}^2}} \right], \quad (2.4)$$

$$n_{\text{c}}(r, z, t) = \frac{\sqrt{2m\mu^3 (1 + \omega_r^2 t^2)}}{3\pi\omega_r a \hbar^2} \max \left[ 1 - \frac{x^2}{r_{r,c}^2} - \frac{z^2}{x_{z,c}^2}, 0 \right]^{3/2}.$$

Here  $\omega_r, \omega_z$  are the angular trap frequencies of the radial and axial direction respectively,  $a$  is the scattering length, and  $t$  is the expansion time when trap is turned off. Below  $T_c$   $\mu$  in the thermal column density is zero and above  $T_c$  the condensate column density is zero since the condensate is non-existent [8]. The spatial widths of the thermal cloud and condensate,  $x_{i,\text{th},c}$  with  $i = r, z$ , are defines as

$$k_{\text{B}} T = \frac{m}{2} \left( \frac{\omega_i^2 x_{i,\text{th}}^2}{1 + \omega_i^2 t^2} \right), \quad (2.5)$$

$$\mu = \frac{1}{2} m \omega_r^2 x_{i,c}(0)^2.$$

Here  $i = r, z$  so  $x_{i,\text{th}}$  are the spatial widths of the thermal cloud and  $x_{i,c}(0)$  is the spatial width of the condensate at  $t = 0$ . Eq. 2.5 shows that the temperature of the system can be extracted from the spatial width of the thermal cloud and the chemical potential is extracted from the width of the condensate if there is a BEC otherwise it is contained in the Boltzmann distribution function. Since a BEC does not expand homogeneously the spatial widths of a cigar shaped condensate expands according to its trapping frequencies

$$x_{r,c} = x_{r,c}(0) \sqrt{1 + \omega_r^2 t^2}, \quad (2.6)$$

$$x_{z,c} = x_{z,c}(0) \left[ 1 + \frac{\omega_r^2}{\omega_z^2} \left( \omega_r t \arctan(\omega_r t) - \ln(\sqrt{1 + \omega_r^2 t^2}) \right) \right].$$

By inserting Eq. 2.6 into Eq. 2.5 one can extract the chemical potential in a expansion experiment.

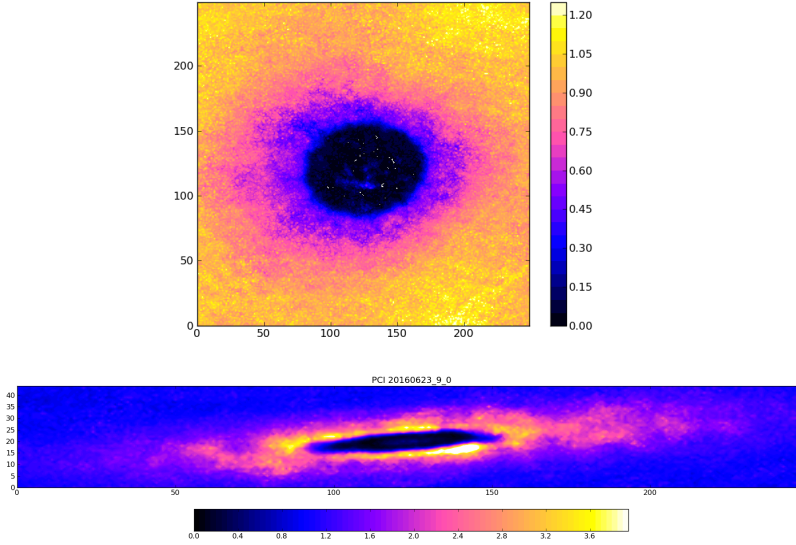


**Figure 2.1:** The top graph shows an absorption picture in top imaging with an expansion time of 10 ms. The bottom graph show a PCI picture of the BEC in-situ.

### 2.5.2 Phase-Contrast Imaging

The other imaging method available is PCI. In the current constructed setup PCI can only be applied in top imaging. The principle is to use the refractive index of the atomic cloud to induce a phase shift, therefore the phase difference of the light from the cloud and background will result into a intensity profile which can be observed. The atomic cloud is projected onto the camera using two lenses which result in the magnification factor of 3. The first lens is focused at the atomic cloud and the second lens is focused on the camera to give a sharp image of the cloud. In between the second lens and the camera there is phase plate with a edged hole (called phase spot) with a diameter of  $50 \mu\text{m}$ . The background light will be focused onto the phase spot, the depth of the phase spot will result into a phase shift. The phase spot in the imaging setup is chosen to give a  $\theta = \pi/3$  phase shift.

The use of refractive index of the cloud means the probe light cannot be resonant which means that the PCI method is non-destructive. This opens up possibilities like making multiple images of the same BEC in-situ. It also demands that density of the cloud must be high enough to induce a significant phase shift. Whereas in absorption imaging one could image the atomic cloud far above  $T_c$  in side imaging, PCI can only image the cloud near  $T_c$  and below. But also in expansion experiments absorption imaging is favorable over PCI due to the fast expansion of atomic cloud.

The transmittance of the image is

$$\frac{I}{I_0} = 3 - 2 \cos(\theta) + 2 \cos(\theta - \phi) - 2 \cos(\phi), \tag{2.7}$$

$$\phi = \frac{k\alpha}{2\epsilon_0} n_{\text{column}}.$$

The phase  $\phi$  depends on the column density  $n_{\text{column}}$  defined in Eq. 2.4. Here  $k = 2\pi/\lambda$ ,  $\alpha$  is the complex polarizability, and  $\epsilon_0$  is the electric permittivity in vacuum. Fig. 2.1 shows an example for both absorption imaging and PCI.

### 3 Supersonic Flow

To generate Čerenkov wakes in BECs means that an object must travel faster than the phase velocity of the dispersive medium. This gives rise to two questions on generating Čerenkov wakes: How fast is the phase velocity of the medium and how can an object move faster than this phase velocity? For generating any type of excitations in a BEC the speed limit is the Landau critical velocity. Though not all excitations will generate observable Čerenkov wakes, but sound-like excitations (long wavelength phonons) can create such density modulations. Thus the main goal will be to move an object (a focused laser) through the BEC faster than the speed of sound.

#### 3.1 Sonic Speed Limit

Čerenkov wakes are generated when the speed of an object is above the speed of sound. For the case of a boson gas below  $T_c$  this is not so trivial since there exist two sounds: a density fluctuation mainly in the thermal cloud (or normal fluid) called first sound and a density fluctuation mainly in the BEC cloud (or superfluid) called second sound. The general definition for first and second sound is that the first sound is a almost pure density wave and second sound is a almost pure thermal wave, but for a boson gas the density and temperature fluctuation is coupled due to weak interaction. The result is that the specific heat at constant pressure  $C_p$  and volume  $C_v$  not equally large. Therefore the second sound has a significant impact on the density function on the superfluid making the separation between density and thermal wave propagation impossible. To simplify the idea lets consider a pure BEC at non-zero temperature in the Thomas-Fermi limit. Now one can write down a simplified hydrodynamic equation for the perturbed density  $\delta n$  from the time-dependent Gross-Pitaevskii equation where the kinetic pressure term is neglected:

$$\frac{\partial^2 \delta n}{\partial t^2} = \nabla (c^2(\mathbf{r}) \nabla \delta n). \quad (3.1)$$

$$c_B(\mathbf{r}) = \sqrt{\frac{4\pi\hbar^2 a}{m^2} n(\mathbf{r})}. \quad (3.2)$$

The density perturbation is given relative to its equilibrium as  $\delta n = n - n_{\text{eq}}$  and for a boson gas at  $T = 0$  the speed of sound in the superfluid is equal to the Bogoliubov speed of sound. Eq. 3.2 shows that it is proportional to the square root of the local density of the condensate.

When taking into account the normal fluid the speed of sound derivate from Eq. 3.2. Two models on the sound propagation in a two fluid system are available, namely the Zaremba, Griffin, and Nikuni (ZGN) model and the Landau model. Both predict that below  $T_c$  the speed of second sound is slower than  $c_B$ , until  $T$  is near the

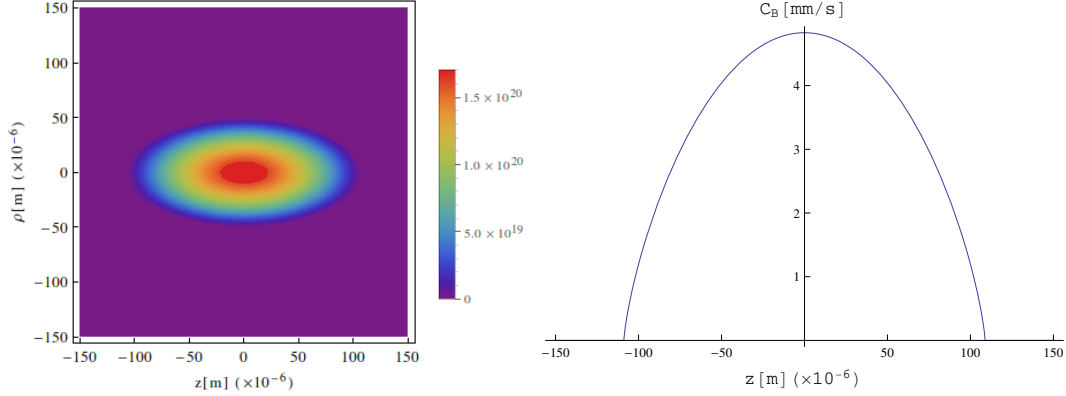


**Figure 3.1:** The left graph shows the density distribution of a pure condensate for  $\mu = 2.8$  kHz. The right graph shows the sound velocity distribution.

temperature of an avoided crossing. There first and second sound interchange their characteristics and superfluid sound reaches  $c_B$  exponentially and the normal fluid vanishes. Between  $T$  near the avoided crossing and  $T_c$  the speed of second sound is theoretically and experimentally determined at roughly  $0.9 - 0.95c_B$  [9].

The distribution of the Bogoliubov speed of sound can be determined using Eq. 3.2 and the column density for the condensate in Eq. 2.4. The density and the sound speed distribution of plotted in Fig. 3.1. The chemical potential used to calculate the distribution is the averaged value of expansion measurements done the same day as the Čerenkov wake experiments. The expansion measurements were done in absorption imaging with an expansion time of 10 ms. The result is  $\langle \mu \rangle = 2.8$  kHz. The BEC will move in the axial direction, it is then important to know the sound speed in that axes. For this we define the radial average density as  $\langle n \rangle(z) = n(0, 0, z)/2$ . By plugging the radial average density into Eq. 3.2 we get a top speed of 4.8 mm/s. This will be used as the speed of sound of the BEC throughout this thesis. The approximation is made that this speed is constant over the BEC since Fig. 3.1 show a strong immediate rise in  $c_B$  towards the peak value. Also as will be shown later on the velocities of the moving BEC will be much larger than this speed of sound therefore effects due to low  $c_B$  at the edges will be negligible.

### 3.2 Gaussian Barrier Setup

The setup is split into two parts. The first part consist of the Ventus which generates green laser light, a telescope, an acousto-optic modulator (AOM), a shutter and a fiberport, where the light is directed via a optical fiber to the second part of the setup. The green laser is generated by a solid-state Continuous Wave laser that emits light at 532 nm with a maximum power of 1.5 W. Explanation on operating the laser and re-calibration can be found in the operating manual [10]. The telescope consists of

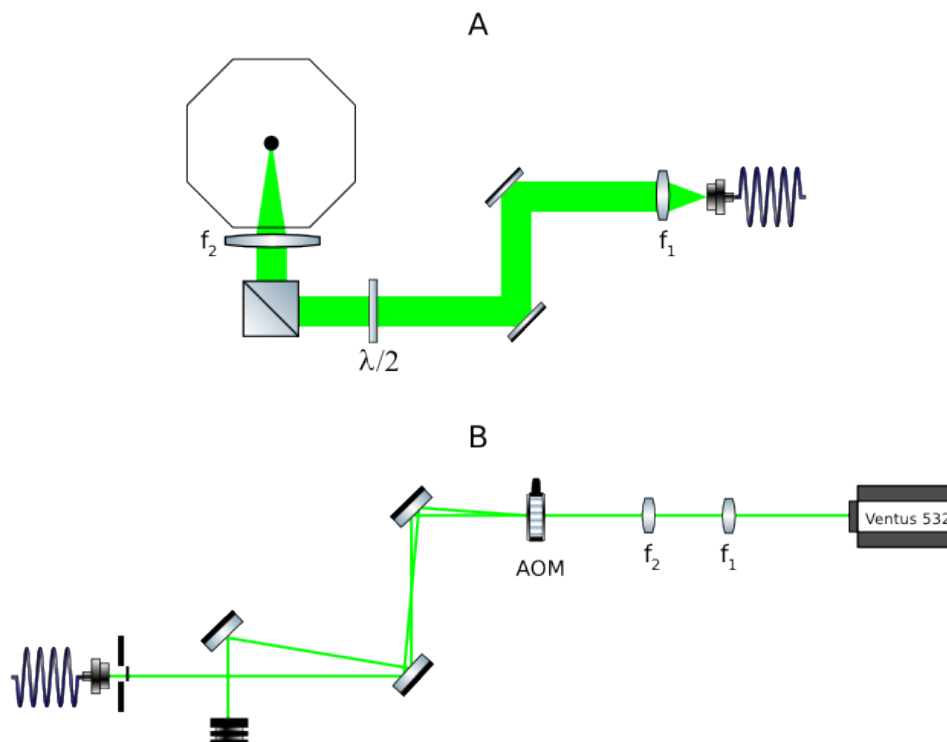


**Figure 3.2:** A schematic overview of the setup. Part (A) and (B) are separate parts linked by an optical fiber. Part (A) is the main part with the vacuum chamber and part (B) is where the Ventus is stationed.

two lenses with a focus of 75 mm and  $-40$  mm, respectively. The combination yields a magnification of 1.875. The reason is to shrink the beamspot so that the cut-off of the entering the AOM can be minimized resulting in an increase of efficiency. The function of the AOM is to quickly switch the light on and off since the shutter closing time is too slow. The shutter is implemented as an extra feature to make sure no light enters the fiberport.

The second part of the setup consists of a fiberport, two lenses, a  $\lambda/2$  plate and a polarizing beam splitter cube. The first lens with a focus of 75 mm is for collimating the beam, since the fiberport has a numerical aperture of  $na = 0.12$ . The radius of the collimated beam can be calculated with the following equation:

$$na = \sin(\theta) = \frac{r}{\sqrt{r^2 + f^2}} \tag{3.3}$$

$$\Rightarrow r = \sqrt{\frac{na^2 f^2}{1 - na^2}}.$$

This yields a radius of 9 mm. The  $\lambda/2$  plate is implemented to maximize the efficiency that is split by the beam splitter cube. The final lens with a focus of 250 mm will create a tight focus on the BEC.

### 3.2.1 Gaussian Beam Optics

To create a tight focus onto the BEC one must first know what the important parameters are and how they relate with each another. This becomes clear by looking at the following equations:

$$w_0 = \frac{\lambda}{\pi} \left( \frac{f}{w_L} \right), \tag{3.4}$$

$$DOF = \frac{2\lambda}{\pi} \left( \frac{f}{w_L} \right)^2. \tag{3.5}$$

Where  $w_0$  and  $w_L$  denotes the radius of the Gaussian at the focus and lens respectively, the radius is defined as the length where intensity is decreased to  $1/e^2$  from its peak value.  $\lambda$  is the wavelength which is in our case 532 nm,  $f$  is the focus length of the lens and  $DOF$  (depth of focus) as the distance where the area of the beam grows to  $\sqrt{2}$  with respect to the area at the focus.

For this setup the focus length is 250 mm and  $w_L$  is 18 mm, therefore  $w_0$  is 4.7  $\mu\text{m}$  and  $DOF$  is 261  $\mu\text{m}$ . The  $DOF$  is large compared to the radial size of the BEC

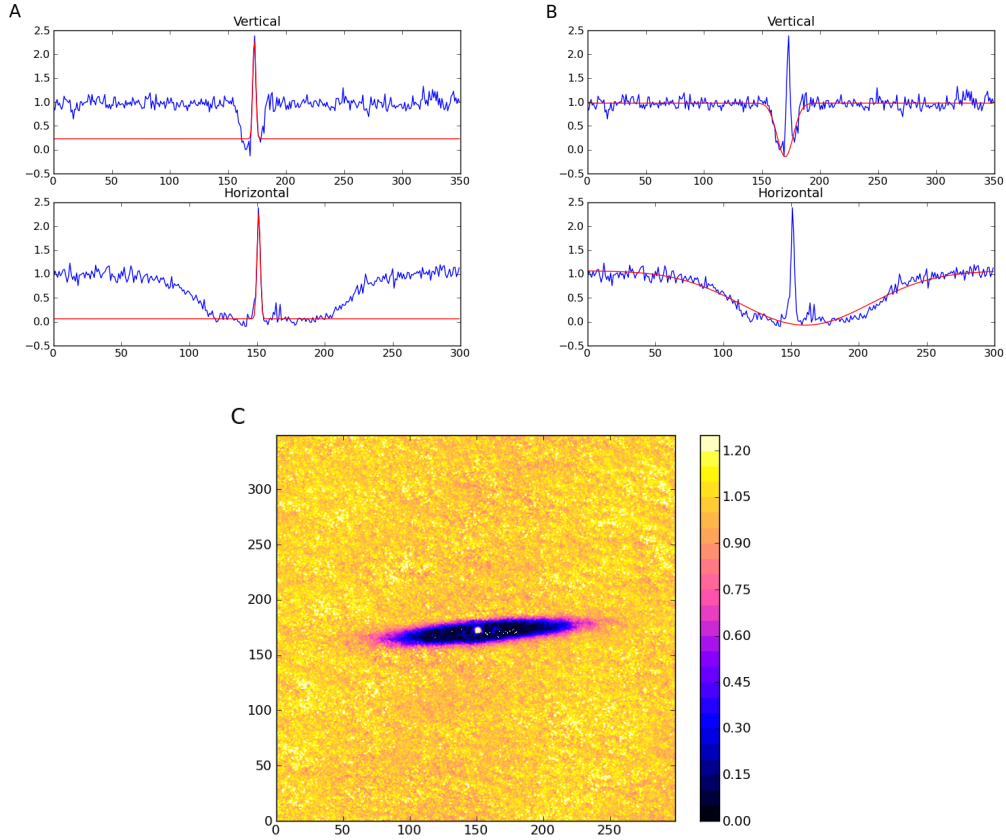


**Figure 3.3:** The top two graphs is the intersection of the BEC center where the hole is caused by the dimple. The Gaussian dimple (A) and BEC (A) are fitted separately. The bottom picture (C) shows the absorption image of the dimple in the BEC.

within the expansion time of 10 ms which is within the timespan of the experiments of interest.

### 3.2.2 Atom-Laser Interaction

When an atom is subjected to light, the electric field induces an atomic dipole moment that oscillates with the driving frequency of the electric field. The strength of the dipole moment is dependent on the electric field and the atomic polarizability. The interaction potential is dictated by the time averaged dipole moment and electric field given by

$$U_{\text{dip}}(\mathbf{r}) = -\frac{1}{2}\langle \mathbf{p}\mathbf{E} \rangle = -\frac{\text{Re}[\alpha]}{2\epsilon_0 c} I(\mathbf{r}), \quad (3.6)$$

Power	4.6 mW
Diameter ( $2\sigma$ )	$10.0 \pm 0.2 \mu\text{m}$
$U_{\text{dip,peak}}$	$19.7 \mu\text{K}$
$\Gamma_{\text{sc}}$	$0.5 \text{ s}^{-1}$

**Table 3.1:** The properties of the focused laser beam that was shown in Fig. 3.3.

$$\Gamma_{\text{sc}}(\mathbf{r}) = \frac{\langle \dot{\mathbf{p}} \mathbf{E} \rangle}{\hbar\omega} = \frac{\text{Im}[\alpha]}{\hbar\epsilon_0 c} I(\mathbf{r}). \quad (3.7)$$

Eq. 3.6 and 3.7 are expressions for the atom-field interaction potential and scattering rate of a dipole in an external field  $\mathbf{E}$ .  $\mathbf{p}$  is the dipole moment  $\mathbf{p} = \alpha\mathbf{E}$ , with  $\alpha$  as the complex polarizability, and  $I(\mathbf{r})$  is the external field intensity. The two equations show that the potential depends on the intensity and the real part of  $\alpha$ , whereas the scattering rate depends on the intensity and imaginary part of  $\alpha$ .

To calculate the potential and scattering rate it is important to know what  $\alpha$  is. Consider the Lorentz's classical oscillator model of an electron ( $m_e$ ) with charge  $-q$  bound to the atom-core with an eigenfrequency ( $\omega_0$ ) corresponding to the optical transition frequency and a damping rate ( $\Gamma_\omega$ ) corresponding to the radiation of the oscillating electron according to the Larmor equation. The equation of motion is given by

$$\ddot{x} + \Gamma_\omega \dot{x} + \omega_0^2 x = -\frac{qE(t)}{m_e}. \quad (3.8)$$

Since the green laser is far-detuned with respect to the resonance frequency, the scattering rate will be very low and the saturation of the excited state is negligible. This is good, because a significant difference between the quantum model and the classical model is the possibility of the excited state getting overpopulated due to high intensities of the external laser field. When this happens the classical model is no longer valid since it does not include higher and lower states. Therefore it is a good approximation, Eq. 3.6 and Eq. 3.7 becomes

$$U_{\text{dip}}(r) = -\frac{3\pi c^2}{2\omega_0^3} \left( \frac{\Gamma}{\omega_0 - \omega} + \frac{\Gamma}{\omega_0 + \omega} \right) I(r), \quad (3.9)$$

$$\Gamma_{\text{sc}}(r) = \frac{3\pi c^2}{2\hbar\omega_0^3} \left( \frac{\omega}{\omega_0} \right)^3 \left( \frac{\Gamma}{\omega_0 - \omega} + \frac{\Gamma}{\omega_0 + \omega} \right)^2 I(r), \quad (3.10)$$

$$\text{with } I(r) = \frac{2P}{\pi w_0^2} e^{-\frac{2r^2}{w_0^2}}. \quad (3.11)$$

$\Gamma$  is the natural linewidth.  $\omega_0$  is the resonant frequency and  $I(r)$  is the intensity of the external field for a Gaussian profile. Eq. 3.9 and Eq. 3.10 shows that there are two frequencies of  $\omega$ , a resonant contribution which is  $\omega = \omega_0$  and a counter-rotating term  $\omega = -\omega_0$ . The detuning of the green laser is  $|\omega_0 - \omega| = 3.4 \times 10^{14}$  which is 20 times smaller than the counter-rotating term and 10 times smaller than  $\omega_0$ , the difference in magnitude is large enough to apply the rotating-wave approximating where the counter-rotating term can be neglected and  $\omega/\omega_0 \approx 1$ . Eq. 3.9 and 3.10 are simplified to

$$U_{\text{dip}}(r) = -\frac{3\pi c^2}{2\omega_0^3} \left( \frac{\Gamma}{\omega_0 - \omega} \right) I(r), \quad (3.12)$$

$$\Gamma_{\text{sc}}(r) = \frac{3\pi c^2}{2\hbar\omega_0^3} \left( \frac{\Gamma}{\omega_0 - \omega} \right)^2 I(r).$$

Fig. 3.3 shows the image of the BEC interaction with a blue-detuned focused laser beam. The laser beam has a power of 4.6 mW, the hole is fitted with a Gaussian function and the diameter of the hole is defined as two times the width  $w_0$  as defined in Sec. 3.2.1. The size of the hole is shown in table 3.1. This is in reasonably close agreement with the value calculated. Reasons for why it is larger than the expected size could be that the focus is not perfectly aligned at the BEC, also due to the nature of the setup there are always weak diffraction patterns present in the form of Airy disks where the higher orders may contribute to the size of the hole depending on the amount of power of the laser beam.

The peak potential and scattering rate generated by the laser assuming the beam waist of  $10 \mu\text{m}$  are also shown in table 3.1 and having the defect potential peak at  $19.7 \mu\text{K}$  means that it is well above the critical temperature for Bose-Einstein Condensation and can be seen as a hard barrier by the condensate.

### 3.3 Oscillations in the Magnetic Trap

To move to a BEC with respect to the focused laser we chose to move the BEC while keeping the laser stationary. This method requires the magnetic trap to manipulate its field on trapped atomic cloud. In the Thomas-Fermi limit the trapping potential near the center of the MT field has a harmonic form

$$U = U_0 + \frac{m}{2} [\omega_\rho^2(x^2 + y^2) + \omega_z^2 z^2], \quad (3.13)$$

the radial and axial trap frequencies are  $\omega_\rho = 102 \text{ Hz}$  and  $\omega_z = 15 \text{ Hz}$ , respectively. If the BEC is placed away from its trap center it will gain potential energy. Therefore by

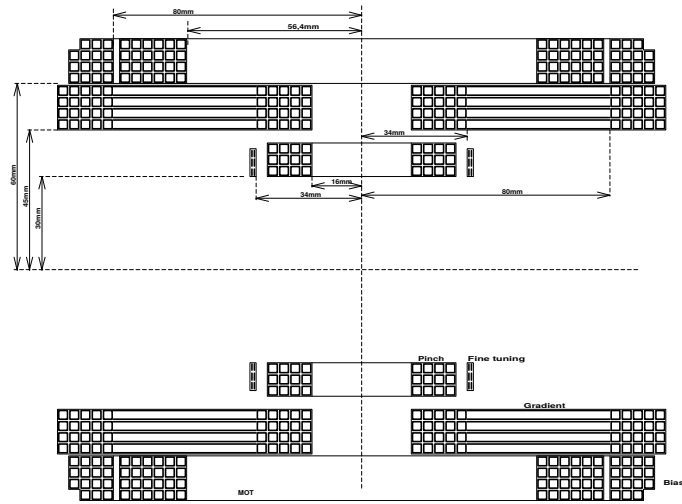


Figure 3.4: The cross section layout of the magnetic coils.

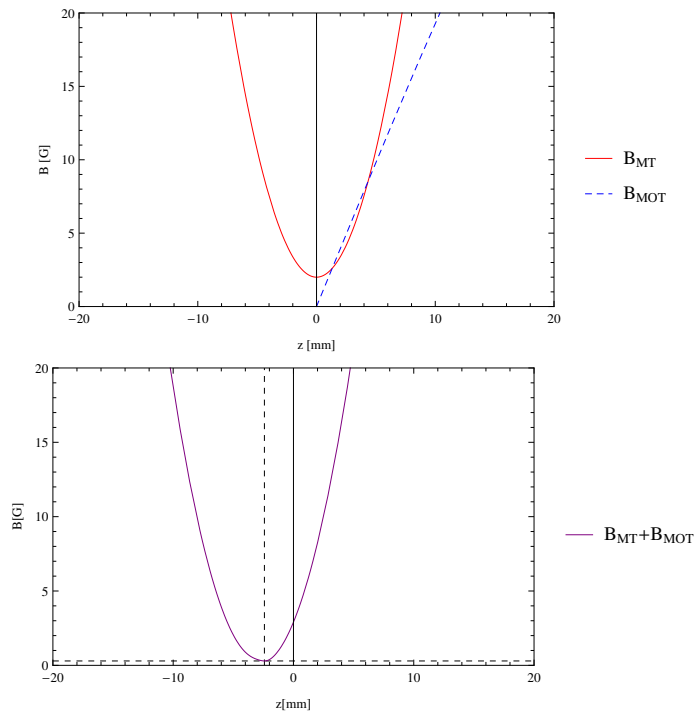


Figure 3.5: The top graph shows the magnetic field strength of the MOT and MT coils in the axial direction. The bottom graph shows the magnetic field strength of the MOT and MT coils combined.

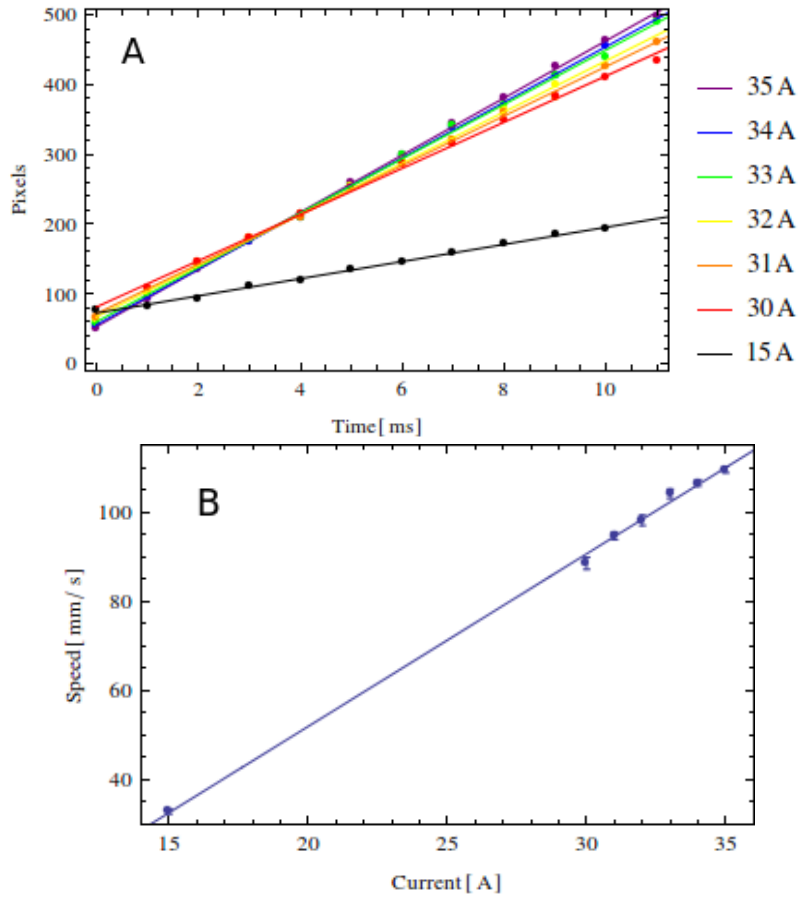
letting the BEC fall in its suspended position it will oscillate in the trap according to the trap frequency, all the potential energy will be transferred to kinetic energy when it reaches the trap center. Fortunately the configuration of the MOT coils allows us to move the magnetic field minimum in the axial direction. By slowly increasing the strength of the MOT field, the BEC can be moved adiabatically away from its original trap center. When the MOT field is switched off, the BEC finds itself back in its original trap potential, but displaced by a distance from the center. The velocity in the trap is given by the conservation of energy,  $v(z) = \omega_z z$ .

Fig. 3.4 shows the cross section layout of the magnetic coils. The coils are hollow square shaped copper wires with glassfiber isolation. Note that one full loop consist of two squares (one on the upper-half and one at the lower-half). The most important contributions to the magnetic trap are the gradient coils for radial confinement and the pinch/bias coils for axial confinement. The gradient coils are situated on two sides of the vacuum chamber and each side is configured like a cloverleaf. The pinch and the bias (in series) are also both situated on two sides, where their polarities are opposite from each other. A shunt is implemented with the pinch/bias so that the bias can be bypassed by up to 125 A. The MOT coils is in an anti-Helmholtz configuration and will generate a gradient field contribution in the axial direction. The gradient will displace the magnetic minimum from its original trap center which is shown in Fig. 3.5.

The magnetic field of the MOT coils in the axial direction can be calculated by assuming that each loop can be approximated as a closed circle and the geometrical shape of the wire is negligible with respect to its distance to the trap center. Thus we approximate that the current will flow at the center of a square wire with radius  $R_i$  and distance from the center plane  $d_j$ . There are a total of 24 loops on each side, see Fig. 3.4. The dimensions of the wires including the isolation layer is  $3.9 \text{ mm} \times 3.9 \text{ mm}$ . The magnetic field generated by the MOT coils is calculated using equation

$$B_{\text{MOT}}(z) = \sum_{i=1}^4 \sum_{j=1}^6 \frac{\mu_0 I}{2R_i} \left[ \frac{1}{\left(1 + \left(\frac{z}{R_i} - \frac{d_j}{2R_i}\right)^2\right)^{3/2}} - \frac{1}{\left(1 + \left(\frac{z}{R_i} + \frac{d_j}{2R_i}\right)^2\right)^{3/2}} \right]. \quad (3.14)$$

During experiments the magnetic coils are operating at 362 A for the gradient coils and 200 A for the pinch/bias coils. The MOT coils generating the gradient field plotted in Fig. 3.5 is at 20 A. During the experiment the MOT coils will generate currents up to 35 A.



**Figure 3.6:** Graph (A) shows the position of the center of the BEC versus time. The fit yields the results of the velocity of the BEC (see table 3.2). Graph (B) shows the velocity versus current.

Current	Velocity	Mach
15 A	$32.9 \pm 0.6$ mm/s	6.9
30 A	$88.5 \pm 1.3$ mm/s	18.4
31 A	$94.6 \pm 0.9$ mm/s	19.7
32 A	$98.1 \pm 1.2$ mm/s	20.4
33 A	$104.1 \pm 1.0$ mm/s	21.7
34 A	$106.5 \pm 0.7$ mm/s	22.2
35 A	$109.5 \pm 0.7$ mm/s	22.8

**Table 3.2:** The fit results from Fig. 3.6 and its respective Mach number.

### 3.4 Measurements

The velocities generated are experimentally determined using PCI with a time interval of 3 ms between each shot. To increase the time resolution extra measurements are done where a delay of 1 and 2 ms is implemented before the imaging sequence. This increases the time resolution to 1 ms between each data point.

The current through the MOT coils for the experiment are set between 30 - 35 A and one at 15 A to check for a linear behavior. After switching off the MOT coils the BEC will be pulled back to the magnetic trap center and when the edge reaches the center, the MT is turned off completely so that it can expand freely with a constant velocity moving in the axial direction. Using PCI its position in time is determined as is shown in Fig. 3.6(A). The velocities extracted from the fit is shown in table 3.2. From Fig. 3.6(B) it is clear that the velocity generated by the MOT field is linear with respect to the current. This is due to the fact that the MOT field is linearly dependent on the current resulting in a linear displacement. The velocity generated due to the displacement is also linear, so clear why the velocity goes linear with the current. 35 A is the stable limit that the power supply of the MOT coils can deliver. Going above this value resulted in an unstable magnetic field causing a rippling effect on the edges of the BEC.

## 4 Čerenkov Wakes

The theory on Čerenkov radiation was originally based on charged particles in a dielectric medium where the excited modes are electromagnetic waves radiating outwards in a cone analogous to the Mach cone. This theory can be expanded upon on other natural phenomena and it is quite remarkable that the basic features resemble that of the Čerenkov radiation [11, 12]. In the general case one must construct the dispersion relation which will contain information on what kind of excitations will be emitted in that particular medium. Then by imposing the Čerenkov condition onto the dispersion relation disturbances in the medium due to the excited modes can be studied.

### 4.1 Bogoliubov-Čerenkov Theory

Lets start with the standard time-dependent Gross-Pitaevskii equation

$$i\hbar \frac{\partial \Psi(\mathbf{r}, t)}{\partial t} = \left( -\frac{\hbar^2 \nabla^2}{2m} + V(\mathbf{r}) + g|\Psi(\mathbf{r}, t)|^2 \right) \Psi(\mathbf{r}, t). \quad (4.1)$$

Applying the Bogoliubov approximation with minor adjustment to the external potential  $V(\mathbf{r})$  will result in an expression for the perturbed density. This expression contains the wake patterns that can be interpreted as the Čerenkov emission of the Bogoliubov excitations. The first minor adjustment is the external potential, by adding an extra defect term which will move with a velocity  $\mathbf{v}$  with respect to the condensate. For explaining the theory the barrier will assume the defect to be a delta potential. Also the condensate will be assumed to be homogeneous and uniformly flowing at a constant speed, this means the only external potential present will be that of the defect, and the defect itself will induce a weak density perturbation. The dispersion relation for the elementary excitations can be calculated from the linear Bogoliubov approximation

$$\omega(\mathbf{k}) = \mathbf{v} \cdot \mathbf{k} \pm \sqrt{\frac{\mathbf{k}^2}{2m} \left( \frac{\hbar^2 \mathbf{k}^2}{2m} + 2gn_0 \right)}. \quad (4.2)$$

The full derivation of the method is shown in App. A. The second term is the Bogoliubov dispersion relation for  $\mathbf{v} = 0$  which is defined as  $\Omega(\mathbf{k})$ . Eq. 4.2 shows the behavior of the excitations in a BEC where at long wavelengths it behaves sound-like with a linear spectrum and for short wavelength it goes quadratic like a free-particle spectrum with a mean-field contribution. This dispersion behavior is crucial for the existence of superfluidity in the BEC.

Now lets consider moving the BEC throught a small barrier  $V_d \delta(\mathbf{r})$ . The introduction

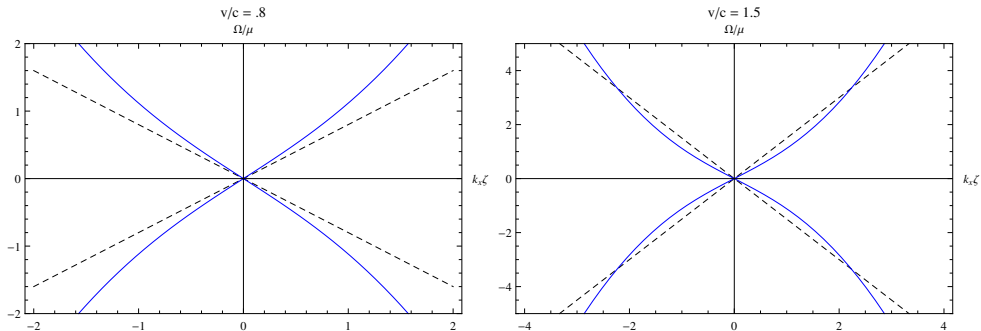


**Figure 4.1:** A 1D representation of the two terms of the denominator of Eq. 4.3, where the velocity  $v$  is 0.8 times the speed of sound on the left and 1.5 on the right. The dashed line is the function  $\mathbf{v} \cdot \mathbf{k}$  and the solid line is  $\Omega(\mathbf{k})$ .

of the Čerenkov condition (explained in App. B) to the linear Bogoliubov approximation will result to the following expression for the density:

$$\tilde{n} = 1 + 4V_d \int \frac{\frac{\hbar^2 \mathbf{k}^2}{2m}}{(\mathbf{v} \cdot \mathbf{k})^2 - \frac{\mathbf{k}^2}{2m} \left( \frac{\hbar^2 \mathbf{k}^2}{2m} + 2g|\psi_0|^2 \right)} e^{i\mathbf{k} \cdot \mathbf{r}} \frac{d\mathbf{k}}{(2\pi)^D}. \quad (4.3)$$

$\tilde{n}$  is the normalized density  $n/n_0$ . The integral of Eq. 4.3 shows that there are values for  $\mathbf{k}$  where the denominator is zero. This realization is very important for understanding Čerenkov wakes. Equating the denominator to zero,  $(\mathbf{v} \cdot \mathbf{k})^2 - \frac{\mathbf{k}^2}{2m} \left( \frac{\hbar^2 \mathbf{k}^2}{2m} + 2g|\psi_0|^2 \right) = 0$ , this will actually recover the Čerenkov condition in the restframe of the BEC. Then by taking the square root of the expression will return to Eq. 4.2. Fig. 4.1 shows the two terms plotted separately for a moving defect of  $v = 1.5c$ .  $\Omega$  is the second term in the denominator,  $\mu$  is the chemical potential, and  $\zeta$  is the healing length defined as  $\zeta = \sqrt{\hbar^2/m\mu}$ . The points where the two lines cross correspond to the the denominator being zero. Fig. 4.2 shows the 2D plane in  $k$ -space where the two terms cross each other, line in Fig. 4.2 is called the locus of the excited modes whose energy is  $\omega = 0$ . It has an aperture angle  $\theta$  indicating the Čerenkov cone in  $k$ -space at  $k \ll 1$ , which is shown at the dashed lines. The relative group velocity, defined as  $\mathbf{v}'_g = \nabla_{\mathbf{k}}(\mathbf{v} \cdot \mathbf{k} - \Omega(\mathbf{k}))$  moves in the direction normal to the locus.

Fig. 4.2 shows that there is only a crossing of the two terms at  $\mathbf{k} \neq 0$  if the velocity of the barrier with respect to the BEC is faster than the speed of sound defined as  $c = \sqrt{gn/m}$ . If this condition is not met then the locus will be empty and no modes that is resonant with  $\omega(\mathbf{k}) = 0$  will be excited, although if the velocity is above the Landau critical velocity it will excite other modes. Only if the barrier reaches velocities of Mach ( $M = v/c$ ) one or higher it can excite the mode which can create Čerenkov wakes.

Lets now concentrate on solving the integral of Eq. 4.3. First to simplify the integral

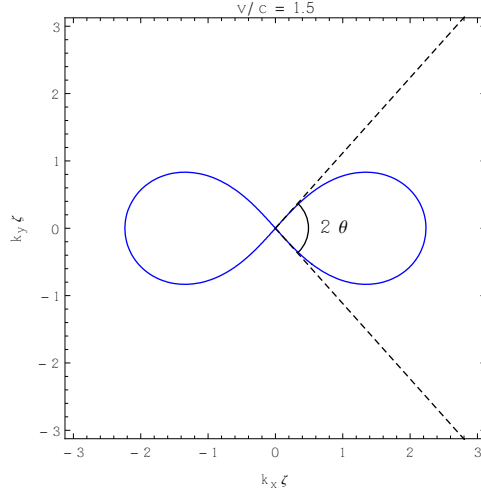


**Figure 4.2:** The 2D shape of the locus with velocity of 1.5 time the speed of sound. The solid line is the path where the values for  $\mathbf{k}$  correspond to the excited modes. The dashed lines is the tangent of the locus at  $k_x, k_y = 0$ .

lets set  $\hbar, m, g, |\psi_0|^2$ , and  $V_d$  to 1, also the integral will be evaluated for the 2D case.

$$\delta\tilde{n} = 2 \int \frac{\mathbf{k}^2}{(\mathbf{v} \cdot \mathbf{k})^2 - \mathbf{k}^2(\mathbf{k}^2/4 + 1) + i0} \frac{d\mathbf{k}}{(2\pi)^2}. \quad (4.4)$$

An extra term is now added which will shift the poles an infinitesimal amount in the positive imaginary direction. This is done to add the boundary condition that at  $t = -\infty$  no excitations resonant with the Bogoliubov mode is present or with other words that the potential barrier is switched on very slowly such that it will not create any excitations. Then by transforming the Cartesian coordinates to polar coordinates the equation becomes

$$\begin{aligned} k_x &= k \cos(\theta), & k_y &= k \sin(\theta), \\ x &= r \cos(\eta), & y &= r \sin(\eta), \end{aligned} \quad (4.5)$$

$$\delta\tilde{n} = -\frac{2}{\pi^2} \int_{-\pi}^{\pi} \int_0^{\infty} \frac{k e^{ikr \cos(\theta-\eta)}}{k^2 - k_0^2 - i0} dk d\theta,$$

with  $k_0 = 2\sqrt{(M \cos(\theta))^2 - 1}$ .

Here it is assumed that the defect moves in the  $\hat{x}$  direction with a velocity  $M$  times the speed of sound, simplifying  $\mathbf{v} \cdot \mathbf{k} = Mk \cos(\theta)$ . Then one can perform a contour integral of  $k$  by first separating it into a sine and cosine. By doing this Eq. 4.5 is

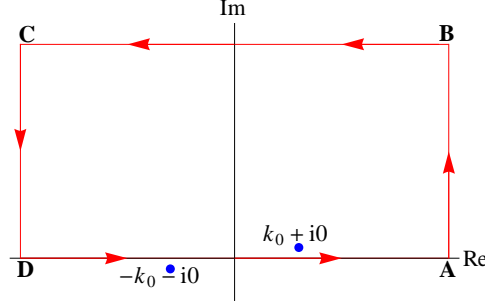


**Figure 4.3:** The red line is the chosen contour path which encircles all positive  $k_0$  poles. The blue dot shows such a pole for a given value  $\theta$  and  $M$ .

split into a even and odd function.

$$\int \frac{ke^{ik\alpha}}{k^2 - k_0^2 - i0} dk \rightarrow \int \frac{f(k) + ig(k)}{k^2 - k_0^2 - i0} dk,$$

$$f(k) = ke^{-\alpha \text{Im}[k]} \cos(\alpha \text{Re}[k]), \quad g(k) = ke^{-\alpha \text{Im}[k]} \sin(\alpha \text{Re}[k]), \quad (4.6)$$

$$\text{with } \alpha = r \cos(\theta - \eta).$$

Fig. 4.3 shows the contour path. Point A goes to infinity in the real axes, point B goes to infinity in both real and imaginary axes, point C goes to infinity in the imaginary axes and negative infinity in the real axes, and point D goes to negative infinity in the real axes.

Path A→B is zero due to the fact that  $\text{Re}[k] \rightarrow \infty$ , the denominator due to its quadratic nature will then dominate and with the condition  $\alpha > 0$  the exponential will converge to zero in the limit  $\text{Im}[k] \rightarrow \infty$ . Path B → C is zero only if  $\alpha > 0$  due to the fact that  $\text{Im}[k] \rightarrow \infty$ . Therefore the exponential which is the dominating term goes to zero. Path C → D is zero for the same reason as for path A → B only the limit of  $\text{Re}[k]$  has switched sign. Path D → A is therefore the only remaining path which is not zero. Since  $f(k)$  is an odd function, the integral of  $f(k)$  is zero,  $g(k)$  on the other hand is even. Now by applying the residue theorem Eq. 4.6 becomes

$$h(k) = \oint \frac{f(k) + ig(k)}{k^2 - k_0^2 - i0} dk \rightarrow \int_0^\infty \frac{2ig(k)}{k^2 - k_0^2 - i0} dk = 2\pi i \text{Res}(h(k), k_0), \quad (4.7)$$

$$\text{Res}(h(k), k_0) = i \sin(\alpha \text{Re}[k_0]).$$

On the condition that  $k_0$  is real this is because there exist a region of excluded directions for the group velocity which correspond to the unperturbed region inside

the Čerenkov cone. Also note that Eq. 4.2 contains a  $\pm$  sign. This corresponds to the positive and negative energies of the Bogoliubov excitation. Which can be seen as particle- and hole-like excitations and are images of each other under the transformation  $\mathbf{k} \rightarrow -\mathbf{k}$  and  $\omega \rightarrow -\omega$ . To select the particle-like excitations in the polar coordinate integral means selecting the right interval for the integration over the angle  $\theta$ . For the case of the defect moving in the positive  $\hat{x}$  direction with respect to the BEC means that the right half locus contains the particle-like excitations, see Fig 4.2. The integration limit of  $\theta$  is  $[-\pi/2, \pi/2]$ . The final equation becomes

$$\delta\tilde{n} = \frac{4}{\pi} \int_{-\pi/2}^{\pi/2} \sin(\alpha \text{Re}[k_0]) d\theta. \quad (4.8)$$

Fig. 4.4 shows the result of the density modulation. As mentioned earlier the relative group velocity of the excited mode moves in the direction normal to the locus. And for  $k \ll 1$  where the dispersion is sound-like it has a Čerenkov cone indicated as the dashed line for Fig. 4.2. These modes propagate in the same direction and so the density has concentrated conical sheets in the 2D surface geometry in real space around the direction of  $v'_g$ , Eq 4.9 shows the geometry in  $k$ - and real-space for mode in the sound-like region of  $\Omega = ck$  and from the geometry the equation for the Mach number is deduced [13].

$$k_y^2 = k_x \left( \frac{v^2}{c^2} - 1 \right),$$

$$y^2 = \frac{c^2 x^2}{v^2 - c^2}, \quad (4.9)$$

$$\implies \sin(\phi) = \frac{c}{v} = \frac{1}{M}, \text{ with } M \text{ as the Mach number}$$

## 4.2 Gaussian Potential

The solution given in Eq. 4.8 is for a defect potential that is a delta function. So the focus of the laser is infinitely small. In reality this is impossible and the focus of our laser has a finite radius (see Sec. 3.2.1). So now we implement a Gaussian potential

$$V_d(\mathbf{r}) = \frac{2V_d}{\pi\sigma^2} e^{-\frac{2r^2}{\sigma^2}} \iff \tilde{V}_d(\mathbf{k}) = V_d e^{-\sigma^2 \mathbf{k}^2 / 2}. \quad (4.10)$$

A nice feature of the Gaussian function is that after performing a Fourier transform

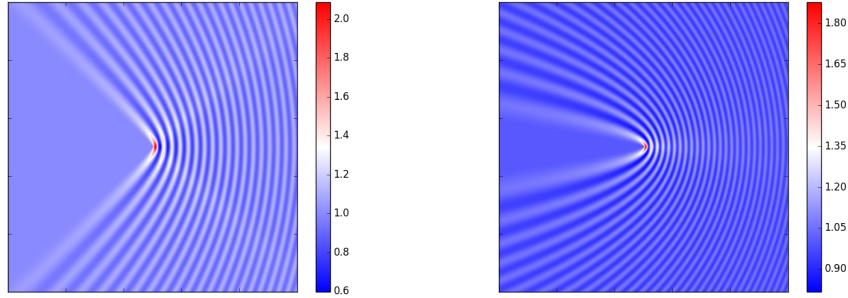


**Figure 4.4:** Density distribution of a BEC moving through a delta potential at Mach 1.5 (left) and Mach 8 (right).

it retains its form as seen in Eq. 4.10. By plugging Eq. 4.10 into Eq. 4.3 will result into the following equation for the perturbed density

$$\delta\tilde{n} = \frac{4}{\pi} \int_{-\frac{\pi}{2}}^{\frac{\pi}{2}} \sin(\alpha \text{Re}[k_0]) e^{-\sigma^2 k_0^2/2} d\theta. \quad (4.11)$$

Eq. 4.11 now also depends on the beam waist  $\sigma$  which will dictate the amplitude and wake patterns in the density. When  $\sigma$  is small The exponent term goes to 1 and the excited wake patterns form according to Fig. 4.4. But when  $\sigma$  increases the exponent grows and starts to dominate over the  $\sin(\alpha \text{Re}[k_0])$  term, therefore it destroys the periodic wake patterns at large distances at the front of the barrier. The suppression of these wake patterns draws closer to the barrier for increasing  $\sigma$  and speed until there is only the zeroth order wake left. Fig. 4.5 shows four situations for increasing  $\sigma$ . The area in front of the potential where the density is relatively higher in respect to the rest of the condensate increases for increasing  $\sigma$  in the opposite direction of the moving condensate. This asymmetry can be explained with the notion that flow around the barrier above the speed of sound result in drag force. This drag force is caused by the pressure difference around potential barrier [14]. Since the barrier moves above the critical velocity means atoms cannot flow frictionless around it. Atoms will accumulate at the front of the barrier due to elastic collisions against the barrier where will fly back in the same direction as the barrier with the same velocity.

### 4.3 Measurements

The measurements were done in the various velocities discussed in Sec. 3.4. To move the BEC away from the the MT center we ramp up the MOT current for 700 ms (see Sec. 3.3). We do this to be sure that the displacement goes adiabatically therefore minimizing any loss that will result from it. After the BEC is displaced we immedi-

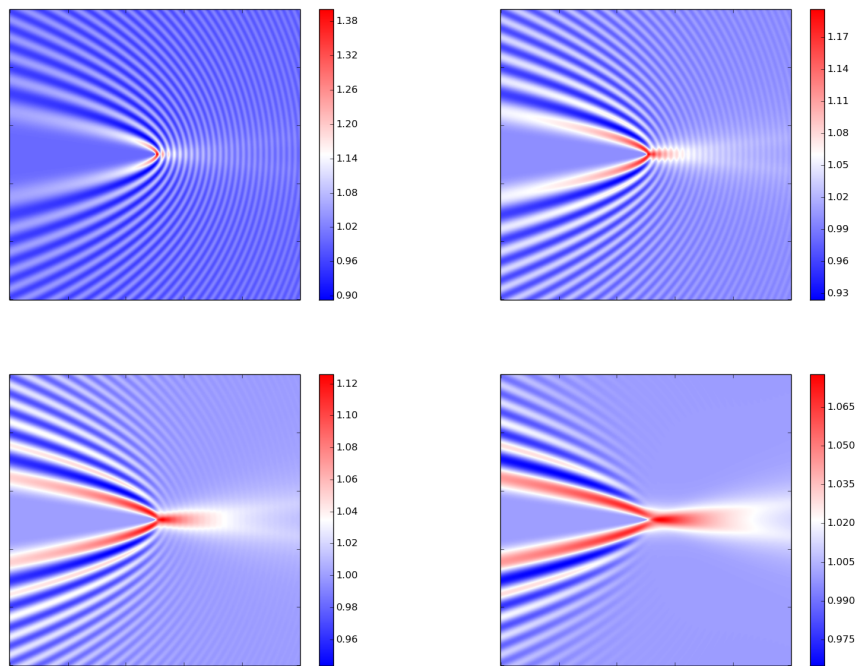


**Figure 4.5:** Density distribution of a BEC moving through a Gaussian potential at Mach 8. The beam  $\sigma$  varies, at the top left  $\sigma = 0.1$ , top right  $\sigma = 0.15$ , bottom left  $\sigma = 0.2$ , and bottom right  $\sigma = 0.3$ .

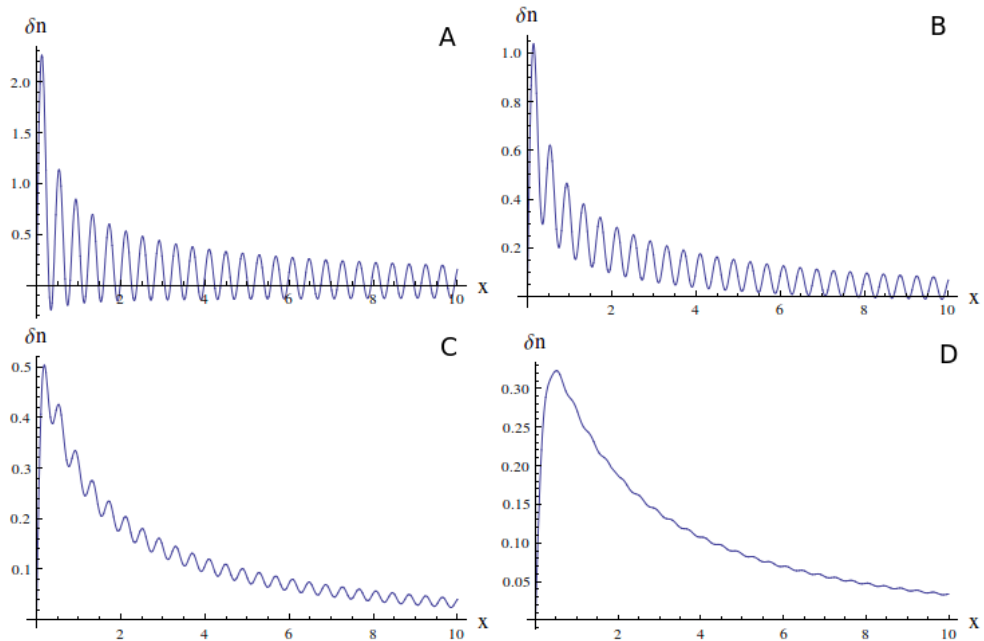


**Figure 4.6:** The horizontal density cross section at the center of the Gaussian potential barrier with a BEC moving at Mach 8. The beam  $\sigma$  varies for (A) a  $\delta$ -function, (B)  $\sigma = 0.1$ , (C)  $\sigma = 0.15$ , and (D)  $\sigma = 0.2$ .

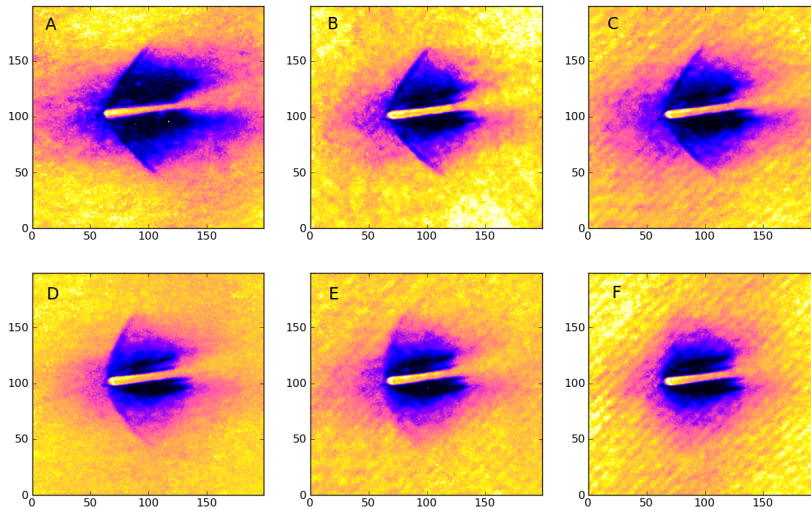


**Figure 4.7:** A BEC moving through a potential barrier with different velocities. (A) has a velocity  $v = 109.5$ , for (B)  $v = 106.5$ , for (C)  $v = 104.1$ , for (D)  $v = 98.1$ , for (E)  $v = 94.1$ , and for (F)  $v = 88.5$ .

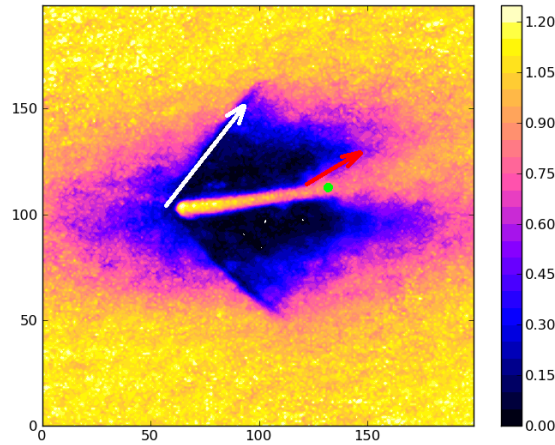


**Figure 4.8:** The white arrow indicates the wake which starts at the beginning of the trail. The red arrow indicates the wake that was created at the end of the trail. The green dot is the estimated position of the potential barrier when the wake at the end was created.

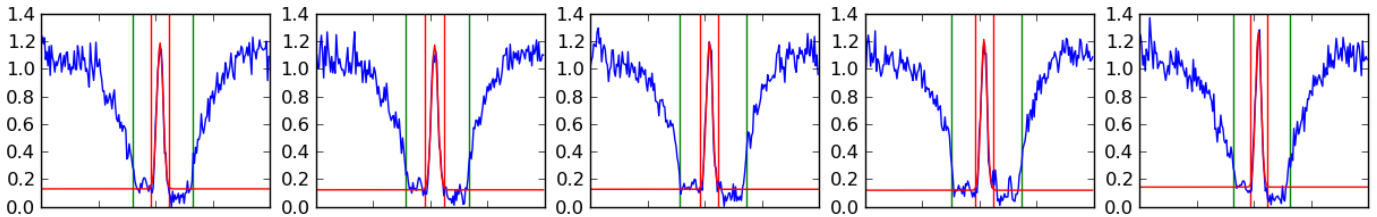


**Figure 4.9:** 5 example cross sections of the pixel column of the image. The sharp drop in signal gives a high contrast for formation of the wake. The trail of the potential barrier is fitted with a Gaussian (shown by the red solid lines). The two vertical red line indicate the region of the Gaussian of  $3\sigma$  width. The green lines indicate the position of the wake.

ately switch of the MOT current, this causes a sudden change in the magnetic field. The BEC will obtain potential energy due to this displacement from the MT field minimum. The result is that it falls back towards the center converting its potential energy to kinetic energy. The time it takes for the edge of the atomic cloud to reach the potential barrier is determined experimentally. This period is found to be 18ms and is found to be the same for all six velocity settings. After 18ms the MT field is turned off and the the atomic cloud is allowed to expand freely while moving through the potential barrier. The expansion time is set to 5ms, after that we probe the event with absorption imaging. Fig. 4.8 shows an example image for all six velocities. From the data shown in the figure we analyze the wakes that is most clear in the picture. This is the wake indicated with the white arrow in Fig. 4.8.

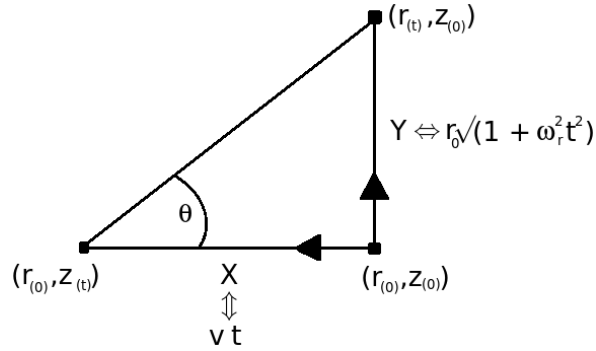


**Figure 4.10:** A schematic drawing on the calculation of the angle gained from the radial expansion of the condensate.

The analysis is done by horizontal cropping the image. In this cropped image where wake is most visible we look at the vertical cross section for each pixel column of the image. Due to the high contrast of the wake, the start of the wake in the cross section is determined using an algorithm which gives an estimated position of the sharp signal drop in the pixel column. We also determine the center position of the trail left by the potential barrier to determine a tilt. The cause of the tilt is that the BEC does not move perfectly horizontal with respect to the picture. We then fit a straight line to the obtained positions of the wake and the center of the trail.

When a BEC is released from its magnetic trap it does not expand homogeneously. The radial expansion velocity goes as  $v_r(t) = r(0)\sqrt{t^{-2} + \omega_r^2}$ . This will contribute to an additional angle increase with respect to the expansion time. Fig. 4.10 shows schematically how the additional angle is calculated. Assume the potential barrier passes an atom with a radial velocity at  $t = 0$ . Excluding the formation of wakes, the barrier will see that atom at  $t = t'$  at an angle

$$\theta = \arctan\left(\frac{r_0\sqrt{1 + \omega_r^2 t^2}}{v_z t}\right). \quad (4.12)$$

Here  $v_z$  is the velocity of the barrier in the axial direction with respect to the atom. This is plotted in Fig. 4.11 for the six velocities. The angle as a function of time for all six velocities shows negligible differences with respect to each other. The figure also shows that for  $t > 2$  ms the radial velocity behaves linearly, this means the additional angle will be constant.

The upper and lower angles are calculated separately with respect to the tilt of the trail and also the averaged angle which is half of the sum of the upper and lower angle. They are plotted in Fig. 4.12 with the angle correction due to the expansion.

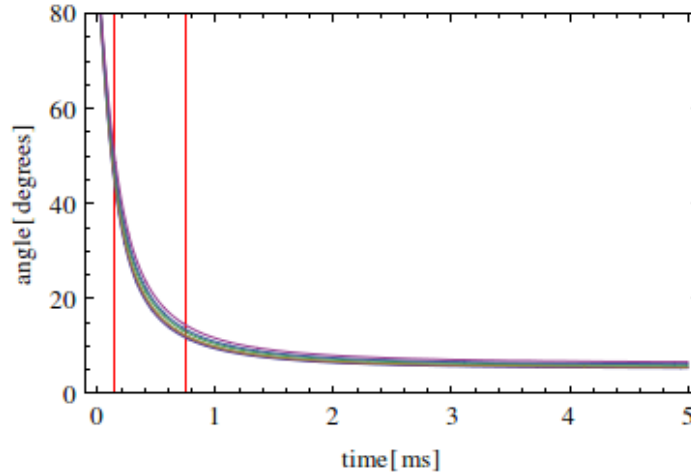


**Figure 4.11:** The angle of a radially expanding atom in the condensate with respect to the object. The graph contains the angle with respect to the expansion time for the four largest velocities. The left line is at  $t = 0.14$  ms and the right line at  $t = 0.75$  ms

The data point with the correction of  $t = 5$  ms is clearly too high from the expected Mach angle. We varied the angle correction for different expansion times and to get close to the theoretical prediction we had to set the expansion time to  $t = 0.14$  ms. This is not realistic which means the predictions by the theory do not correspond to the data.

To try and somehow match the data points we increased the speed of sound from 4.8 to 77 mm/s. The results are plotted in Fig. 4.13 with the corrected expansion time of 5 ms. The data are here in good agreement with the predicted theoretical values.

Finally we also measured the angle of the wake that appears at the end of the trail which is indicated with a red arrow in Fig. 4.8. Since the contrast of this wake is too low we cannot apply the same algorithm to determine the position of the wake. To measure the angle we use an image analysis program called Fiji<sup>1</sup>. The angles are a rough estimate determined using Fiji with an error margin of  $4^\circ$ . The error margins are determined by increasing and decreasing the angle to a value where it seems that the angle stops corresponding to that of the wake. The results are plotted in Fig. 4.14. The uncorrected data set still seems to be high. Then after an expansion time correction of  $t = 0.75$  ms shows that the data is in good agreement with the theory. To be sure we have chosen the correct expansion time we can calculate the position of the barrier in the past since we know that the velocity is constant. By subtracting the 0.75 ms from the 5 ms and multiplying the difference with the respective velocity will result in the distance traveled from the position of 5 ms to 0.75 ms back in time.

<sup>1</sup><http://fiji.sc/>

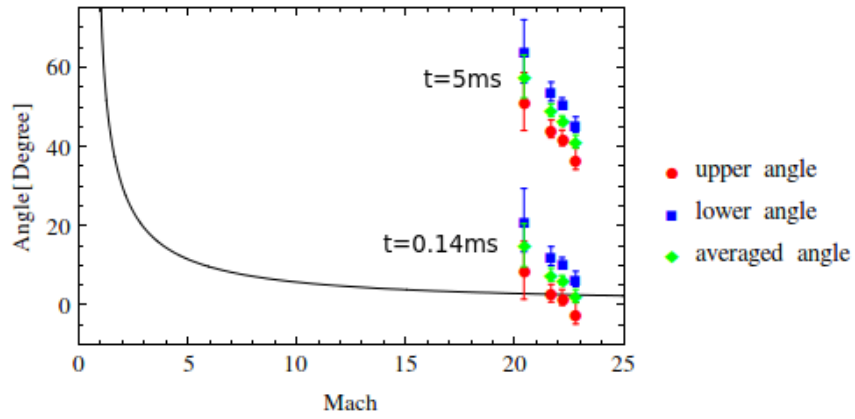


**Figure 4.12:** The data points are the measured angles of the four fastest settings (see Fig. 4.7(A,B,C,D)). The top set of data points are corrected for an expansion time of 5 ms and the bottom set of data points are corrected for an expansion time of 0.14 ms. The solid line is the mach angle  $\sin(\theta) = M^{-1}$ .

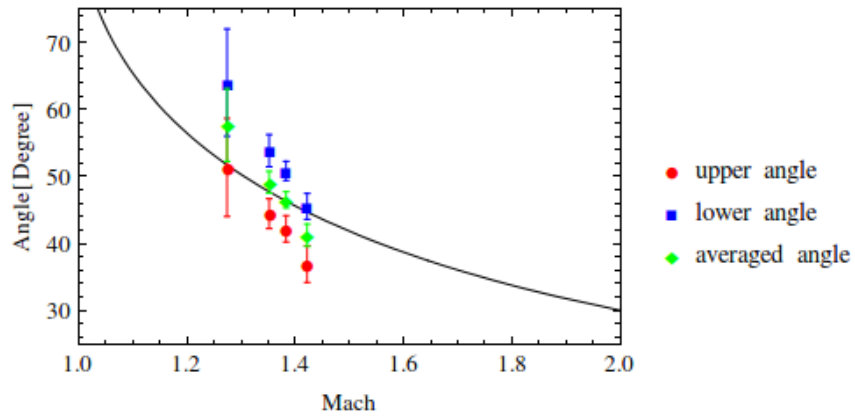


**Figure 4.13:** Here the speed of sound is set to 77 mm/s. The data points are the measured angles of the four fastest settings (see Fig. 4.7(A,B,C,D)). The solid line is the mach angle  $\sin(\theta) = M^{-1}$ .

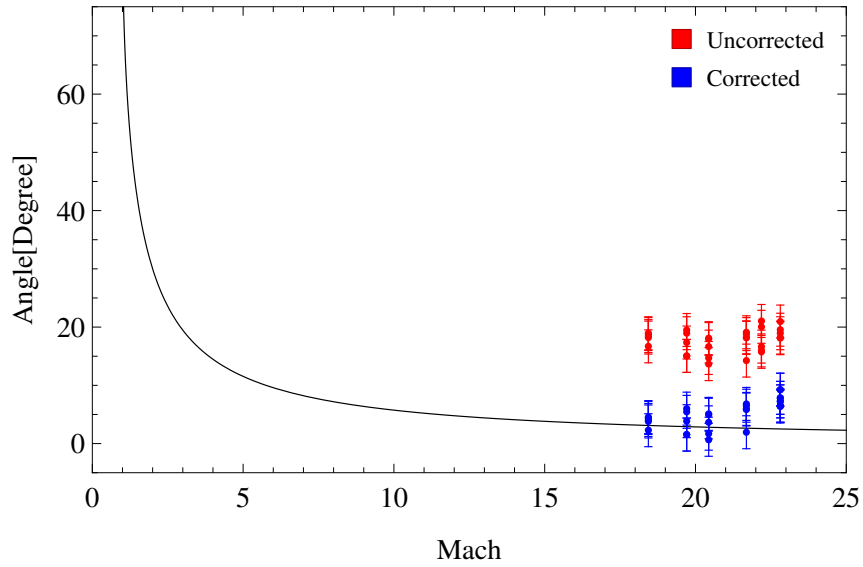


**Figure 4.14:** The measured angles at the tail end. The blue data points are the uncorrected angle values and the red data points are the corrected data points. The solid line is the mach angle  $\sin(\theta) = M^{-1}$ .

This position is indicated with a green dot in Fig. 4.8. The resulting positions are in good agreement with the place where the barrier should be to generate the respective wakes at the end of the trail.

## 5 Discussions

### 5.1 Discussion

The speed of sound of 77 ms which as deduced from changing the speed of sound of the medium so that the data points correspond to theory extremely large. The wakes originating from the beginning of the trail are not wakes of the condensate, but of the normal fluid. The breaching of the speed of sound is therefore not that of second sound, but first sound. But even for normal cloud this is speed of sound is very large. We looked at two models for first sound, namely the ideal Bose gas and the interacting Bose gas model [15]. In the ideal Bose gas the speed of sound depends on the temperature of the system. The temperature of an average BEC measured in a expansion experiment conducted on the same day as the wake experiments was 690 nK. The temperature and speed of sound are related in the following equation:

$$c_1^2 = \frac{\zeta(5/2)}{\zeta(3/2)} \frac{5k_B T}{3m}. \quad (5.1)$$

Here  $\zeta(n)$  is the Riemann zeta function with  $\zeta(5/2) = 1.341$  and  $\zeta(3/2) = 2.612$ . To have a speed of sound of 77 mm/s the system must have a temperature of 19  $\mu$ K. This is an unrealistically large heating for a system of  $T = 690$  nK.

For the interacting Bose gas model the speed of sound is dependent on the local density given as

$$c_1^2 = \frac{n(\mathbf{r})U_0}{m}. \quad (5.2)$$

Here  $U_0$  is the interaction energy defined as  $U_0 = 4\pi\hbar^2 a/m$  with  $a$  as the scattering length. The resulting density for a speed of sound of 77 mm is  $6.49 \times 10^{22} \text{ m}^{-3}$ . The local density here is more than 200 times larger than the peak density of the BEC shown in Fig. 3.1. This is also unrealistically large even if atoms will accumulate at the front of the barrier (see Sec. 4.2). So both models give unsatisfactory results to explaining the extreme rise in the speed of sound. Another explanation is that the wakes at the beginning of the trail does not behave according to the Mach angle.

The accumulation of density shown in Fig. 4.5 was done assuming that the density was homogeneous and the condensate was infinitely large. The rise in density in front of the barrier is therefore not constrained. The predicted asymmetry between the front and back of the barrier was already observed, but the dampening of the wake patterns due to a non-zero beam waist was never observed.

## 5.2 Conclusion

We have successfully been able to give a velocity of up to 109.5 mm/s to the BEC. This equates to a maximum of Mach 22.8 where the speed of sound in the condensate is determined to be 4.8 mm/s. This enabled us to create the right conditions for the Čerenkov wakes to occur. The Bogoliubov-Čerenkov theory gave good insight and understanding on the formation of wake patterns. To conclude, we have successfully observed Čerenkov wakes of the normal and condensate fluid simultaneously. The wake coming from the condensate is at the end of the trail and the wake coming from the normal fluid is at the beginning of the trail.

We now also have a Bogoliubov-Čerenkov theory for a finite sized potential barrier. We predict that the wake patterns will get suppressed for larger velocities and/or larger surface area of the barrier. And the surface area where density increase at the front of the barrier also increase due to the finite size of the barrier.

The measured angle from the condensate is in good agreement with the expected Mach angle. The measured angle from the normal fluid however is only in good agreement for the speed of sound of 77 mm/s. The ideal Bose gas model and interaction Bose gas model cannot explain the large value in speed of sound in the normal fluid. These models describe the normal fluid separately from the superfluid. Models where both fluid interact with each other may contain key insight on the formation of these wakes in the normal fluid.

Although clear wake formations have been observed there is still room for improvement and there are still some open questions on this topic. These will be discussed in the next section.

## 5.3 Outlook

Although the wakes from the normal fluid has a high contrast, the contrast of the condensate wakes are too low to perform proper analysis on the angle. If the image can be made right after the condensate hits the barrier, it is possible to see an early formation of the wakes which should result in much higher contrast. This can best be done by moving the position of the potential barrier back so that after 5 ms the barrier just enters the BEC.

Another problem that arises is the high density of the condensate, this causes the signal in the image to drop to zero. This overshadows all the small patterns of the wake which prevented us from observing the effects predicted in the theory. Fig. 5.1 shows such a picture. The MOT currents are set to 15 A corresponding to Mach 6.9. It is clear from the figure that everything is overshadowed due to the high density. By decompressing the MT one could decrease the density since it is the density that determines the signal output. Detuning the probe is not an option, because the absorption by the condensate is not homogeneous. Measurement done showed various irregular holes while for other parts the signal still drops to zero. If

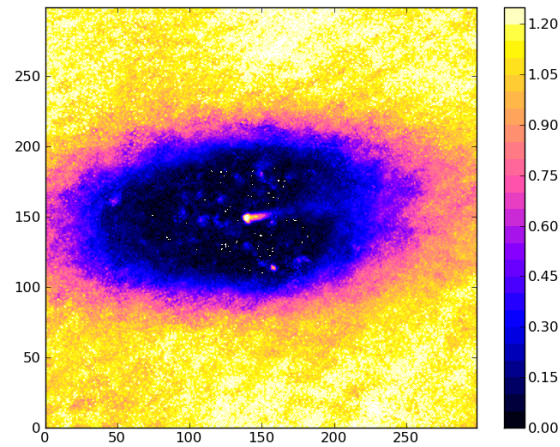


**Figure 5.1:** MOT current of 15 A corresponding to a velocity of 32.9 mm/s (Mach 6.9). The white dot in the center is the potential barrier.

successful wake measurements at lower velocities will be possible and should be done. And PCI may be an option by one must take into account the signal is dependent on the phase difference due to the density which may result in oscillations in the signal. This may form a problem when trying to observe higher order wake patterns in the density.

Finally it is still unclear what kind of mechanism causes the large wake angles at the beginning of the trail. The interactions between the normal and superfluid could play a roll in this since the barrier not only move through the condensate, but also must move past the normal fluid. It is advisable to do wake measurements above  $T_c$ . This will give answers to the wake angles for the normal fluid. The wake angles of the normal fluid should tell us whether the wakes (white arrow of Fig. 4.8) are purely from the normal fluid. Or if there is an underlying mechanism between the normal and superfluid that causes the increase of the wake angle.

## Appendix A : The Linear Bogoliubov Approximation

Consider a small perturbation to the groundstate wavefunction of a uniform gas  $\psi = \psi_0 + \delta\psi$ . Then by implementing it into the Gross-Pitaevskii equation will result into an expression for the small perturbed wave function (note that for this linear approach all quadratic terms of  $\delta\psi$  are neglected)

$$\begin{aligned} i\hbar \frac{\partial \delta\psi}{\partial t} &= -\frac{\hbar^2 \nabla^2}{2m} \delta\psi + V \delta\psi + g (2|\psi_0|^2 \delta\psi + \psi_0^2 \delta\psi^*) \\ -i\hbar \frac{\partial \delta\psi^*}{\partial t} &= -\frac{\hbar^2 \nabla^2}{2m} \delta\psi^* + V \delta\psi^* + g (2|\psi_0|^2 \delta\psi^* + \psi_0^{*2} \delta\psi). \end{aligned} \quad (\text{A.1})$$

Then with the assumption that the perturbed wavefunction has the following form Eq. A.1 can be written in terms of  $u(\mathbf{r})$  and  $v(\mathbf{r})$ :

$$\begin{aligned} \left[ -\frac{\hbar^2 \nabla^2}{2m} + V + 2g|\psi_0|^2 - \mu - \hbar\omega \right] u(\mathbf{r}) - g\psi_0^2 v(\mathbf{r}) &= 0 \\ \left[ -\frac{\hbar^2 \nabla^2}{2m} + V + 2g|\psi_0|^2 - \mu + \hbar\omega \right] v(\mathbf{r}) - g\psi_0^{*2} u(\mathbf{r}) &= 0. \end{aligned} \quad (\text{A.2})$$

$\delta\psi = e^{-i\mu t/\hbar} (u(\mathbf{r})e^{-i\omega t} + v^*(\mathbf{r})e^{i\omega t})$ ,  $e^{-i\mu t/\hbar}$  is the overall phase factor that is chosen to cancel out the effects of the phases of  $\psi_0^2$  and  $\psi_0^{*2}$ . Eq. A.2 is also known as the Bogoliubov equations. If the gas is now assumed uniform so the external potential term vanishes, the chemical potential is then defined as  $\mu = g|\psi_0|^2$ . If the gas also flows uniformly with a constant velocity, the wavefunction can be transformed with respect to the lab restframe:  $\psi(\mathbf{r}, t) \rightarrow \psi(\mathbf{r} + \mathbf{v}t, t)$ . Then by applying the Fourier transform Eq. A.2 can be written as

$$\begin{pmatrix} \left( \frac{\hbar^2 \mathbf{k}^2}{2m} + g|\psi_0|^2 - (\hbar\omega - \hbar\mathbf{k} \cdot \mathbf{v}) \right) & -g\psi_0^2 \\ -g\psi_0^{*2} & \left( \frac{\hbar^2 \mathbf{k}^2}{2m} + g|\psi_0|^2 + (\hbar\omega - \hbar\mathbf{k} \cdot \mathbf{v}) \right) \end{pmatrix} \begin{pmatrix} u_k \\ v_k \end{pmatrix} = 0. \quad (\text{A.3})$$

Here the  $\hbar\mathbf{k} \cdot \mathbf{v}$  term is the result of the partial time derivative term of the transformation with respect to the lab restframe. Eq. A.3 is then only consistent if the determinant of the matrix is zero, this condition will result in a spectrum for elementary excitations:

$$\omega = \mathbf{v} \cdot \mathbf{k} \pm \sqrt{\frac{\mathbf{k}^2}{2m} \left( \frac{\hbar^2 \mathbf{k}^2}{2m} + 2g|\psi_0|^2 \right)}. \quad (\text{A.4})$$

The first term gives rise to the flow of the BEC, the second term is the Bogoliubov dispersion relation for a BEC at rest. In the regime of large wavelengths,  $\mathbf{k} \ll 1$ , Eq. A.4 is linear which indicates that the spectrum is sound-like and the speed of sound in the lab frame is obviously the speed of sound in the BEC restframe plus the velocity of the flowing BEC. In the regime of small wavelengths,  $\mathbf{k} \gg 1$ , Eq. A.4 is parabolic which resembles the spectrum of free particles.

## Appendix B : Čerenkov Condition In BEC

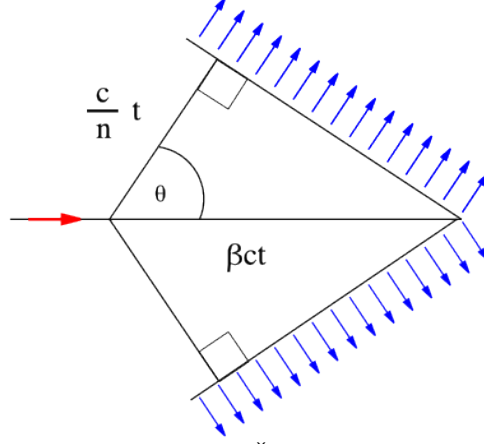


**Figure B.1:** A schematic representation of the Čerenkov effect where the red arrow indicated the direction the particle is moving and blue the direction emitted wave.

In the classical case of Čerenkov radiation let there be a particle that travels with a velocity faster than the phase velocity of light  $c$  in the current medium  $n$ . Then the distance which the particle has traveled from point A to point B is  $x_p = \beta ct$ , with  $\beta = v/c$ . Thus the distance which the electromagnetic wave that was emitted at point A has traveled is  $\frac{c}{n}t$ . If one included every wave emitted on the path of the particle then there would exist a plane wave front where the emitted waves are coherent, see Fig. B.1. This will give the following relation, also known as the Čerenkov condition,

$$\cos(\theta) = \frac{1}{\beta n} = \frac{\omega}{v k} \rightarrow \omega = \mathbf{v} \cdot \mathbf{k}. \quad (\text{B.1})$$

Now lets consider a small perturbation again to the ground state wavefunction, but now also consider adding an extra defect  $V_d(\mathbf{r})$  to the external potential. This changes only the potential term of Eq. A.1 to  $V_d(\mathbf{r})\psi_0$  giving the following equation:

$$i\hbar \frac{\partial}{\partial t} \begin{pmatrix} \delta\psi \\ \delta\psi^* \end{pmatrix} = \begin{pmatrix} -\frac{\hbar^2 \nabla^2}{2m} + g|\psi_0|^2 & g\psi_0^2 \\ -g\psi_0^{*2} & \frac{\hbar^2 \nabla^2}{2m} - g|\psi_0|^2 \end{pmatrix} \begin{pmatrix} \delta\psi \\ \delta\psi^* \end{pmatrix} + V_d(\mathbf{r}) \begin{pmatrix} \psi_0 \\ -\psi_0^* \end{pmatrix}. \quad (\text{B.2})$$

Now by taking the same assumptions and approach as in appendix B. Eq. B.2 can be rewritten as

$$\mathcal{L} \begin{pmatrix} u_k \\ v_k \end{pmatrix} = \tilde{V}_d \begin{pmatrix} \tilde{\psi}_0 \\ -\tilde{\psi}_0^* \end{pmatrix} \quad (\text{B.3})$$

$$\mathcal{L} = \begin{pmatrix} -\frac{\hbar^2 \mathbf{k}^2}{2m} - g|\psi_0|^2 + (\hbar\omega - \hbar \mathbf{k} \cdot \mathbf{v}) & g\psi_0^2 \\ g\psi_0^2 & -\frac{\hbar^2 \mathbf{k}^2}{2m} - g|\psi_0|^2 - (\hbar\omega - \hbar \mathbf{k} \cdot \mathbf{v}) \end{pmatrix} \quad (\text{B.4})$$

$\tilde{V}_d$  and  $\tilde{\psi}_0$  are the Fourier transforms of the defect potential and unperturbed wavefunction. Note that  $\mathcal{L}$  is diagonalizable, so knowing this one can multiply the matrix with its inverse to get the following expression

$$\begin{pmatrix} u_k \\ v_k \end{pmatrix} = \mathcal{L}^{-1} \tilde{V}_d \begin{pmatrix} \tilde{\psi}_0 \\ -\tilde{\psi}_0^* \end{pmatrix}. \quad (\text{B.5})$$

$\mathcal{L}^{-1}$  is the inverted matrix  $\mathcal{L}$ . Eq. B.5 gives the solution for the perturbed wave function in k-space. And the perturbed wavefunction is defined as  $\delta\psi_k = e^{-i\mu t/\hbar}(u_k e^{-i\omega t} - v_{-k}^* e^{i\omega t})$ . Now plugging in the solution of Eq. B.5 into  $\delta\psi_k$  and  $\delta\psi_k^*$  and applying the Čerenkov condition will result into the following two equations:

$$\begin{aligned} \psi_0^* \delta\psi_k &= \tilde{V}_d \frac{\left(-2\frac{\hbar^2 \mathbf{k}^2}{2m}\right) |\psi_0|^2}{\frac{\mathbf{k}^2}{2m} \left(\frac{\hbar^2 \mathbf{k}^2}{2m} + 2g|\psi_0|^2\right) - (\mathbf{v} \cdot \mathbf{k})^2} \\ \psi_0 \delta\psi_k^* &= \tilde{V}_d \frac{\left(-2\frac{\hbar^2 \mathbf{k}^2}{2m}\right) |\psi_0|^2}{\frac{\mathbf{k}^2}{2m} \left(\frac{\hbar^2 \mathbf{k}^2}{2m} + 2g|\psi_0|^2\right) - (\mathbf{v} \cdot \mathbf{k})^2} \end{aligned} \quad (\text{B.6})$$

The assumption is made for the Čerenkov condition in BEC that the excitations behave according to the Bogoliubov dispersion relation. And since the BEC is also moving with a velocity  $\mathbf{v}$ , one need to correct Eq. B.1 accordingly. Therefore  $\omega = 0$  where  $\omega$  is Eq. B.4.

Now the complete density distribution of a moving BEC with the presence of a defect potential can be calculated in steady state. For simplicity the defect potential is chosen to be a delta potential so that  $\tilde{V}_d$  can be taken out of the integral.

$$\begin{aligned} n &= |\psi_0 + \delta\psi|^2 = |\psi_0|^2 + \psi_0^* \delta\psi + \psi_0 \delta\psi^* = n_0 + \delta n \\ \delta n &= 4V_d n_0 \int \frac{\frac{\hbar^2 \mathbf{k}^2}{2m}}{(\mathbf{v} \cdot \mathbf{k})^2 - \frac{\mathbf{k}^2}{2m} \left(\frac{\hbar^2 \mathbf{k}^2}{2m} + 2g|\psi_0|^2\right)} e^{i\mathbf{k} \cdot \mathbf{r}} \frac{d\mathbf{k}}{(2\pi)^D} \end{aligned} \quad (\text{B.7})$$

## References

- [1] E. Cornell. Experiments in rotating, spinning, and shocked becs. KITP conference on Quantum Gases, 2004.
- [2] W. Ketterle. Nobel lecture: When atoms behave as waves: Bose-einstein condensation and the atom laser. *Rev. Mod. Phys.*, 74:1131–1151, Nov 2002.
- [3] E. A. Cornell and C. E. Wieman. Nobel lecture: Bose-einstein condensation in a dilute gas, the first 70 years and some recent experiments. *Rev. Mod. Phys.*, 74:875–893, Aug 2002.
- [4] C. Raman, M. Köhl, R. Onofrio, D. S. Durfee, C. E. Kuklewicz, Z. Hadzibabic, and W. Ketterle. Evidence for a critical velocity in a bose-einstein condensed gas. *Phys. Rev. Lett.*, 83:2502–2505, Sep 1999.
- [5] D.A. Steck. Sodium d line data. *Report, Los Alamos National Laboratory, Los Alamos*, 124, 2000.
- [6] J. Smits. Phase imprinting of vortices in becs using shaped light. Master’s thesis, Utrecht University, 2016.
- [7] C. te Riet. Spatial non-destructive imaging of spin domains in bose-einstein condensates. Master’s thesis, Utrecht University, 2014.
- [8] W Ketterle, DS Durfee, and DM Stamper-Kurn. Making, probing and understanding bose-einstein condensates. *arXiv preprint cond-mat/9904034*, 5, 1999.
- [9] R. Meppelink, S. B. Koller, and P. van der Straten. Sound propagation in a bose-einstein condensate at finite temperatures. *Phys. Rev. A*, 80:043605, Oct 2009.
- [10] <http://www.laserquantum.com/products/detail.cfm?id=25>. More information on the specifications of the laser can be found in the link.
- [11] I. Carusotto, S. X. Hu, L. A. Collins, and A. Smerzi. Bogoliubov-Čerenkov radiation in a bose-einstein condensate flowing against an obstacle. *Phys. Rev. Lett.*, 97:260403, Dec 2006.
- [12] Y. G. Gladush, L. A. Smirnov, and A. M. Kamchatnov. Generation of cherenkov waves in the flow of a boseeinstein condensate past an obstacle. *Journal of Physics B: Atomic, Molecular and Optical Physics*, 41(16):165301, 2008.
- [13] I. Carusotto and G. Rousseaux. *The Čerenkov Effect Revisited: From Swimming Ducks to Zero Modes in Gravitational Analogues*, pages 109–144. Springer International Publishing, 2013.

- [14] R. Onofrio, C. Raman, J. M. Vogels, J. R. Abo-Shaeer, A. P. Chikkatur, and W. Ketterle. Observation of superfluid flow in a bose-einstein condensed gas. *Phys. Rev. Lett.*, 85:2228–2231, Sep 2000.
- [15] C.J. Pethick and H. Smith. *Bose-Einstein condensation in dilute gases*. Cambridge university press, 2002.

## A Acknowledgements

These past few years of my master was quite an experience for me. Working in the Nanophotonics group I had a lot of great memorable moments and want to thank a few<sup>†</sup> people for it. First of all I want to thank Peter van der Straten for supervising me and help me understand and increase my knowledge on the physics of very cold bosons. I like that the talks are always straightforward and direct, but then again everything here is straightforward and direct...and weird sometimes. I then want to thank the "Blije Bosonen" group: Jasper my lab partner in crime (the things we did in the lab), Koen the DJ (the things we did in the club), Broos the clean cut man (the things we did), and Charly the bachelor (the things you did).

Then I want to thank the other part the core master group I started with at the beginning: Robert guitar-meister<sup>†</sup> and originator of the group, Gordian whiz-kid tech-genius and dans-meister, James J-meister beard-meister and always a good time, and of course Marcel meister-meister meister of meistering. Of course there were other master students that joined us later on, but were also great fun. So thank you Jasper (Clarijs), Karindra, Kostas, and Anne for the good time (also thanks Isabelle for the awesome cakes you bake).

The PhD students were always prepared to give a helping hand and were also fun to be around, so thank you Sebas, Arjon, Ole, and Sandy. But I cannot forget their ringleader, Dries van Oosten, who can help you understand a lot of your physics problems, but can also make you very uncomfortable with just his presence.

But where would I be without the technical and mechanic support? Probably here writing my thesis on why everything keeps exploding in my face. So thank you Frits and Dante for all the help with all those electrical hardware, I learn a lot from it. Thank you Cees with all the help with lenses, mirrors, and everything optics you can't learn these things from a textbook. And of course Paul-meister, thanks for making all the stuff for us and all the epic borrels.

Then I want to thank a group that recently joined us in the department, everyone at nanoLINX. Thanks for all the help and good time.

I also want to express my gratitude to the panini-grill<sup>†</sup> and my awesome headphone for helping me work. My heart also goes out to room OL 254, you will always be the first and the best room of the whole building.

And finally the ones I will never forget: my family and parents, the source of my motivation, support, and strength. To them I'm eternally grateful.

---

<sup>†</sup>a lot

<sup>†</sup>Google translate "meister" German-English

<sup>†</sup>R.I.P. 2014-2015